Physics – Uspekhi **50** (8) 793 – 818 (2007)

REVIEWS OF TOPICAL PROBLEMS

PACS numbers: 75.40.Gb, 75.40.Mg, **76.50.+g**

Nonlinear regular and stochastic dynamics of magnetization in thin-film structures

D I Sementsov, A M Shutyi

DOI: 10.1070/PU2007v050n08ABEH006147

Contents

Abstract. Results of investigating nonlinear regimes of the homogeneous precessional dynamics of magnetization in iron – garnet films with various orientations of crystallographic axes and in metallic thin-film structures are presented. Attention is primarily focused on static and dynamic bistabilities, which, under the effect of an ac magnetic field, lead to the magnetization reversal of the systems, bifurcational changes in the magnetization precession amplitude, or the establishment of both stochastic and complex regular (including auto-oscillating) precessional regimes. The bifurcation diagrams considered reveal diverse possibilities of efficiently controlling the nonlinear dynamics of magnetization in thin-film structures by varying external magnetic fields.

1. Introduction

Interest in the nonlinear precession dynamics of magnetization in magnetically ordered crystals cam be explained by the variety of dynamic effects arising under the action of a high-frequency field on dissipative spin systems [1 – 5] and by the possibility of obtaining large angles of magnetization precession and the realization of dynamic chaos and various static and dynamic self-organizing states of magnetic systems [6 – 8]. One of the most suitable objects for the realization and investigation of numerous nonlinear dynamic regimes is thin-film structures, which are widely used in modern integrated-circuit technologies [9].

In recent years, in connection with the active development of new information carriers and methods of information recording, investigations of the dynamic magnetization reversal in thin films [10 – 13], the formation and propagation of an excitation front [14], and the development of homogeneous and structurally inhomogeneous nonlinear dynamic states [15 – 19] have become quite topical. It is understandable that many of the main features of nonlinear regular and stochastic precession regimes should most clearly manifest themselves in homogeneously magnetized structures. In addition, when using nonlinear effects in practice, where the magnitude of the response of a system to an external action is important, it is homogeneous precession dynamics that are preferred. Of special interest are large-amplitude precession regimes, which is related to the possibility of using them for modulating laser radiation, whose efficiency is determined by the magnitude of the precession angle [20 – 23].

It is well-known that in the case of the mutually perpendicular orientation of high-frequency (ac) and static (dc) fields (transverse pumping), there exist two mechanisms of energy transfer from homogeneous precession to spin waves that limit the increase in the precession amplitude [7, 24]. The first mechanism is related to a three-magnon process, in which a magnon with the wave vector $\mathbf{k} = 0$ vanishes and two magnons with wave vectors $\mathbf{k}$ and $-\mathbf{k}$ and the frequency $\omega_k = \omega_0/2$ (where ω_0 is the resonance frequency of uniform precession) arise. The second mechanism is related to a four-magnon process, in which two magnons with wave vectors $\mathbf{k}$

D I Sementsov, A M Shutyi Ul'yanovsk State University,
ul. L. Tolstogo 42, 432970 Ul'yanovsk, Russian Federation
Tel. (7-8422) 32 15 98
E-mail: sementsovdi@ulsu.ru, shuty@mail.ru

Received 14 June 2006; revised 1 March 2007
Uspekhi Fizicheskikh Nauk **177** (8) 831 – 857 (2007)
Translated by S N Gorin; edited by A M Semikhatov

and $-\mathbf{k}$ and the frequency $\omega_k = \omega_0$ appear instead of two magnons with $\mathbf{k} = 0$. When the high-frequency field exceeds a certain threshold field, these processes lead to the development of spin-wave instabilities; as a result, both regular and stochastic nonlinear dynamic regimes can be realized in the related spin system [7, 25 – 28].

To obtain large angles of uniform precession of magnetization, a condition for the suppression of the Suhl instabilities caused by three- and four-magnon interactions should be satisfied. This condition amounts to the requirement that the frequency of the ac field does not exceed the lower value of the frequency $\omega(k)$ in the spectrum of spin waves, i.e., correspond to the bottom of the spin-wave 'band' [1 – 7]. For a thin perpendicularly magnetized layer, the resonance uniform mode of the spin-wave spectrum corresponds to the bottom of the band and, by adjusting the layer thickness, can be moved fairly far from the frequency of the first (nonuniform) spin-wave mode [29]. It is precisely for this reason that the above mechanisms of energy transfer are not realized in perpendicularly magnetized films under the condition $\omega \leqslant \omega_0$. As a result, as the amplitude of the high-frequency (microwave) field increases, no saturation of the resonance in the uniform mode occurs [30] and the specific features of the nonlinear dynamics of magnetization already manifest themselves in the case of uniform precession [31].

One of the manifestations of the nonlinear dynamics of magnetization at large angles of uniform precession is the frequency doubling effect, which occurs in the case of a linear polarization of the high-frequency field. In the case of precession in a transverse microwave field, the consideration is typically limited to this nonlinear effect [24]. But some types of symmetry of the magnetic crystallographic anisotropy lead to the predominant manifestation of the higher harmonics of the basic frequency of precession in the precessional motion of the magnetic moment [32, 33]. The nonlinear coupling of magnetization to an ac field is accompanied by a number of effects caused by a sharp increase in the amplitude of the precession angle [7, 24, 34 – 36]. The dynamic bistability and the related hysteretic field or frequency dependence of the power absorbed by the sample can be attributed to such effects [37 – 39]. Of special interest are the properties of single-crystal thin-film structures near the critical values of the fields that determine the orientational phase transitions at which the change in the magnetization in the layers has a jumplike character. Therefore, determining the most favorable conditions for excitation of various dynamic regimes requires, first and foremost, an analysis of the equilibrium states of the system and the clarification of instability states sensitive to small changes in the parameters of the system and external fields [32, 40].

The nonlinear precession regimes are analyzed in this review using the example of iron – garnet films and metallic multilayer structures. Iron – garnet epitaxial films, which have been quite actively studied in the last few decades, are widely used in various devices of the microwave and optical ranges [20, 41, 42]. The main focus in this review is on an analysis of new precession regimes in (111) and (100) films, i.e., bistable dynamic states, auto-oscillating regimes, and complex regular and stochastic precession. It is shown that the orientation of crystallographic axes essentially determines the trajectory of the precession of the magnetization vector and the frequency ranges responsible for the realization of the auto-oscillatory and stochastic dynamics.

The greater attention being paid lately to the investigation of the ordering features [43 – 45] and resonance properties [46 – 49] of multilayer systems consisting of two or more layers of ferromagnetic metals separated by nonmagnetic metallic spacers is due to the variety of the types of coupling between magnetic moments of the layers [50 – 53] and the unique magnetoresistance properties of these structures [43]. Nonlinear precession regimes, including stochastic ones, can be excited in layered metallic systems by a spin-polarized current passed through the system [54 – 57]. In this review, we restrict ourselves to precession regimes in layered structures with the antiferromagnetic type of interlayer coupling, which arise under the effect of an ac magnetic field that is uniform over the structure.

The dynamics of magnetization in a uniformly magnetized thin layer are generally described by the Landau – Lifshitz equation, which in a spherical coordinate system is written as the set of equations [24]

$$\dot{\varphi} M \sin\theta = \gamma \frac{\partial F}{\partial \theta} - \frac{\lambda}{M} \frac{1}{\sin\theta} \frac{\partial F}{\partial \varphi} ,$$
$$\dot{\theta} M = -\frac{\lambda}{M} \frac{\partial F}{\partial \theta} - \gamma \frac{1}{\sin\theta} \frac{\partial F}{\partial \varphi} , \tag{1}$$

where γ is the gyromagnetic ratio and λ is the dissipation parameter. The free-energy density for an individual magnetic layer is written as

$$F = -\mathbf{M}(\mathbf{H}+\mathbf{h}) - 2\pi M^2 \sin^2\theta + F_{\mathrm{a}}(\theta,\varphi) + F_{\mathrm{u}}(\theta,\varphi) , \tag{2}$$

where $\mathbf{M}$ is the magnetization vector, whose direction is determined by the polar angle θ referenced to the normal to the film, and by the azimuthal angle φ; $\mathbf{H}$ and $\mathbf{h}$ are the external dc and ac magnetic fields; and F_{a} and F_{u} are the contributions determined by the energy of magnetocrystalline anisotropy and by the energy of anisotropy induced during film growth, respectively. Solving Eqn (1) permits finding the time dependence of the magnetization orientation in a given geometry and for a given time dependence of the applied fields. In this review, we present a unified analysis (from the standpoint of the formalism used) of the nonlinear dynamics of magnetization in various thin-film magnetic structures, which is based on the study of solutions of Eqn (1).

2. Low-amplitude precession and orientational dynamic jumps in (111) iron – garnet films

Epitaxial iron – garnet films are single-crystal layers with a cubic crystal lattice. For (111) films, the crystallographic axis [111] is assumed to coincide with the x axis directed along the normal to the film surface, the $[11\bar{2}]$ and $[\bar{1}10]$ axes are taken to coincide with the y and z axes, and the angles θ and φ are referenced to the respective axes x and y. With this orientation of the crystallographic axes, the density of the free energy of magnetocrystalline anisotropy is determined by the expression

$$F_{\mathrm{a}} = K_1 \left(\frac{1}{4} \sin^4\theta + \frac{1}{3} \cos^4\theta + \frac{\sqrt{2}}{3} \sin^3\theta \cos\theta \cos 3\varphi \right), \tag{3}$$

and the density of the free energy of growth-induced anisotropy is written as

$$F_{\mathrm{u}} = K_{\mathrm{u}} \sin^2\theta , \tag{4}$$

where K_1 and K_u are the respective constants of magnetocrystalline and growth-induced anisotropy. In what follows, the external dc and ac magnetic fields are assumed to be mutually orthogonal ($\mathbf{H} \perp \mathbf{h}$).

As follows from the above relations, a substantial effect on the dynamics of magnetization in precessional motion, along with the orientation and magnitude of the magnetizing field and with the fields of growth-induced and magnetocrystalline anisotropy, is also exerted by the polarization, the amplitude, and the initial phase of the microwave field. At low amplitudes of the microwave field ($h \ll H_{\text{eff}}$, where H_{eff} is the effective magnetic field) at a frequency $\omega = \omega_r$, a linear ferromagnetic resonance occurs at which all precession angles are small and the time dependences $\theta(t)$ and $\varphi(t)$ can be found from the equations of motion linearized with respect to small deviations of the magnetization from the equilibrium position. In this case, the frequency of the resonance precession of the magnetic moment with respect to its equilibrium orientation is determined by the expression

$$\omega_r = \gamma H_{\text{eff}} = \frac{\gamma}{M \sin\theta} \left(F_{\theta\theta} F_{\varphi\varphi} - F_{\theta\varphi}^2 \right)^{1/2}, \tag{5}$$

where the magnitudes of the second derivatives of the free energy density are taken at for the equilibrium angles θ_0 and φ_0 obtained from the respective conditions $\partial F/\partial\theta = 0$ and $\partial F/\partial\varphi = 0$. With an increase in the amplitude of the microwave field and, correspondingly, with an increase in the precession angle, the contribution of the higher harmonics of the principal frequency of precession to the dynamics of magnetization increases, and the nutation motion of the vector $\mathbf{M}$ becomes essential. In this case, in solving Eqns (1), the linear approximation becomes insufficient and the main features of the precessional motion can be analyzed in detail, with all the parameters that determine the state of magnetization in the film taken into account, only on the basis of numerical methods.

In what follows, in considering iron–garnet films, we restrict ourselves to the case of a dc field $\mathbf{H}$ directed perpendicularly to the film surface. With the anisotropy constants K_u and K_1 corresponding to the equilibrium orientation of the vector $\mathbf{M}$ along the normal to the film ($\theta_0 = 0$), the frequency of the resonance precession is written as $\omega_r = \gamma H_{\text{eff}}(0)$, where the effective field is

$$H_{\text{eff}}(0) = H - 4\pi M + \frac{2}{M} \left(K_u - \frac{2}{3} K_1 \right). \tag{6}$$

We assume that the ac field is linearly polarized and lies in the yz plane. In this case, there exist several regimes of precessional motion of the magnetization, determined by the magnitude of the dc field H (or by the precession frequency ω).

To reveal the specific features of the precessional motion of the vector $\mathbf{M}$, it is necessary to determine the spatial energy relief specified by the function $F(\theta, \varphi)$. The $F(\varphi)$ dependence has the period $2\pi/3$, in accordance with the positions of the magnetizing field and three crystallographic axes $\{100\}$. For the direction $\varphi = \theta = 0$ (the vector $\mathbf{M}$ is parallel to the normal to the film) and the magnitude of the magnetizing field $H > H_0$, the $F(\theta)$ dependence has a local minimum, which becomes more clearly pronounced with increasing H.

To investigate the above dependences and perform a further analysis, we used parameters close to those of a real iron–garnet film, $4\pi M = 214.6$ G, $\gamma = 1.755 \times 10^7$ (Oe s)$^{-1}$, $\lambda = 3 \times 10^6$ s^{-1}, $K_u = -10^3$ erg cm^{-3}, and $K_1 \approx -10^3$ erg cm^{-3} [41, 58]. The magnitude of H_0 is determined from Eqn (6) under the condition $H_{\text{eff}}(0) = 0$; for the structure chosen, we obtain $H_0 = 245$ Oe. Apart from a minimum along the direction of the normal, there are also three local minima, at the angles $\varphi = 0°$, $120°$, $240°$ and $\theta \approx 35-41°$. With an increase in the magnetizing field, these minima become somewhat shifted toward the normal, become less pronounced, and vanish at $H \approx 279$ Oe.

Analysis [32, 59] shows that at sufficiently small magnetizing fields and low frequencies corresponding to the condition of linear resonance (for the film under investigation, these are $H < 279$ Oe and $\omega_r < 4 \times 10^8$ s^{-1}), the precession axis coincides with the normal only at small amplitudes of the microwave field ($h \leqslant 0.04$ Oe). The precession amplitude in this case is a few degrees ($\phi \approx 2°$). The trajectory of the magnetization motion substantially differs from a circular one already at $h \approx 0.04$ Oe because of the nutation motion of $\mathbf{M}$ with a predominant contribution from the third harmonic of the precession frequency. With an increase in the microwave field amplitude, the magnetization deviates during the precessional motion toward one of the three directions (depending on the orientation of the field $\mathbf{h}$ in the yz plane and on its initial phase), which is determined by the corresponding local minima of the free-energy density with $\theta \neq 0$. In a time $\tau \leqslant 500$ ns, the magnetization starts precessing (about the direction toward which it becomes deviated) over a stationary trajectory with an average amplitude $\langle\phi\rangle \leqslant 3°$.

Below, we present the results of a numerical solution of Eqns (1) that characterize the dynamics of the precessional motion in the film under investigation. Figure 1a displays the yz projections of the normalized magnetic moment $m_\alpha = M_\alpha/M$, $\alpha = y, z$, which changes its initial orientation under the effect of a microwave field, thereby leading to the establishment of one of the four above-described stationary dynamic regimes. The magnitude of the dc field was chosen to be equal to $H = 260$ Oe, which corresponds to a linear resonance precession with the frequency $\omega_r = 1.12 \times 10^8$ s^{-1}. The high-frequency field has the amplitudes $h = 0.04$ Oe (curve *0*) and 1.5 Oe (curves *1–3*) and a zero initial phase. The orientational angles, which are referenced to the y axis, take the values $\varphi_h = 0°$, $200°$, and $270°$ (curves *1–3*, respectively). For the precession of the magnetic moment about the normal (curve *0*), the initial phase is unimportant. The dashed lines in Fig. 1a divide the yz plane into three sectors corresponding to the values of the orientational angle φ_h of the high-frequency field $\mathbf{h}$ at the initial instant at which the precession of $\mathbf{M}$ about the corresponding direction is established. When the initial phase is equal to π, i.e., when the field changes sign at the initial instant, the distinguished regions of the angles φ_h are shifted by $180°$. In the region of the boundary between the sectors, a jump by $240°$ first occurs; upon a further increase in the angle φ_h, a transition to the missed position occurs, with the dynamic regime subsequently remaining in that position until the next changeover of the angular sectors [32]. With a further increase in the dc field H, the three minima of $F(\theta, \varphi)$ located at an angle to the normal vanish; only a precession with the axis oriented along the normal to the sample surface is realized.

Above, we considered cases of a resonance relation between the magnetizing field and the frequency [Eqn (6)]. The other dynamic regimes are realized under conditions differing from the resonance. In the range of magnetizing fields with boundary values $H_\pm \approx H_0 + \tilde{H} \pm \Delta H$, a linearly polarized ac field of a small frequency ($\omega/2\pi < 10^6$ Hz) leads

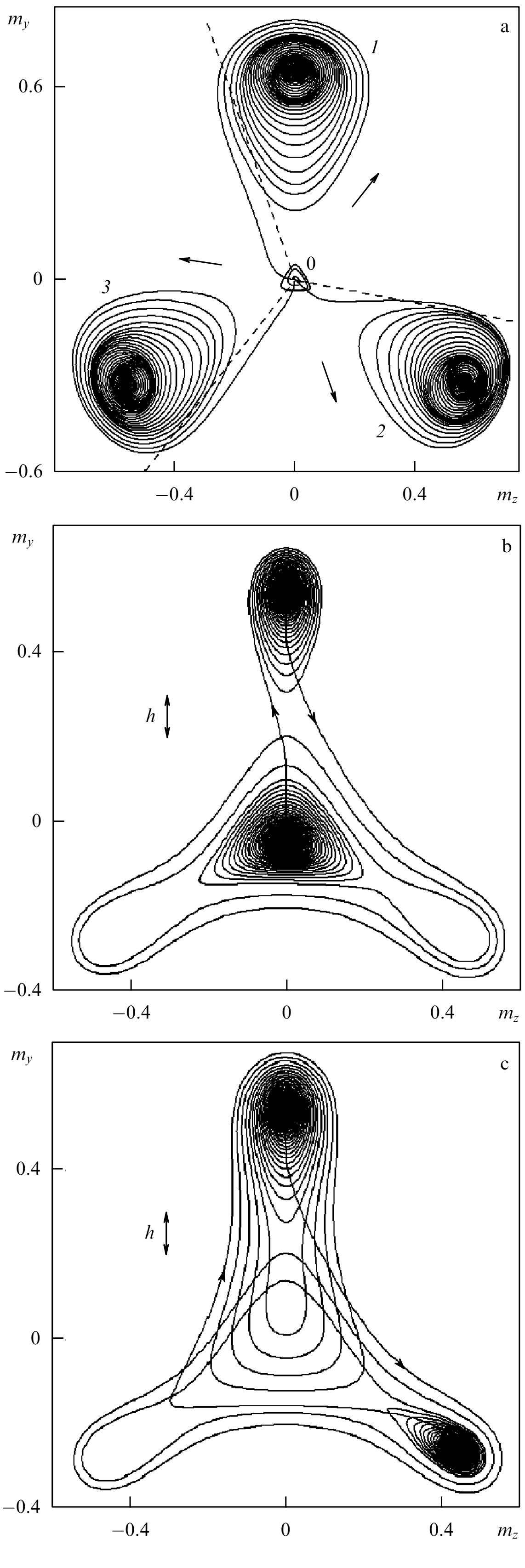

Figure 1. *yz* plane projections of the normalized magnetic moment: exiting, under the effect of a microwave field, into one of four low-amplitude dynamic regimes (a), and executing dynamic jumps (b, c).

to dynamic orientational jumps of the magnetic moment between two or three (of four) equilibrium orientations (Fig. 1a) [60]. The magnitude of $\widetilde{H}$ depends on the growth-induced anisotropy constant; at $K_u = 0$, -10^3, -3×10^3, -5×10^3, and -10×10^3 erg cm^{-3} with the other parameters corresponding to the above-considered structure, we have $\widetilde{H} \approx 37, 24, 12, 7$, and 0 Oe, respectively. The magnitude of ΔH increases as the induced anisotropy field and the ac field amplitude increase; at $h = 1$ Oe and $K_u = -3 \times 10^3$ and -5×10^3 erg cm^{-3}, we have $\Delta H = 2.6$ and 3.0 Oe, respectively; at $h = 2$ Oe and $K_u = -10^3$, -3×10^3, and -5×10^3 erg cm^{-3}, we have $\Delta H = 1.2$, 4.1, and 6.1 Oe, respectively; at $h = 1$ Oe and $K_u = -10^3$ erg cm^{-3}, these regimes are absent. Thus, to obtain these regimes at small amplitudes of the ac field, structures with large fields of the growth-induced anisotropy must be used.

Various regimes of orientational dynamic jumps can be realized, consisting in the following transitions of the magnetization: between the equilibrium direction oriented along the normal to the structure and equilibrium directions with polar angles closest to the orientational angle of the ac field; between the latter and one of the other two equilibrium directions not coincident with the normal; and between three equilibrium directions, one of which is oriented along the normal. At sufficiently large amplitudes of the ac field, several narrow alternating ranges of the values of the magnetizing field corresponding to various regimes of jumps occur.

Figure 1b shows *yz* projections of the normalized magnetic moment executing dynamic jumps in the first (Fig. 1b) and second (Fig. 1c) of the above regimes under the effect of an ac magnetic field with the amplitude $h = 2$ Oe, frequency $\omega/2\pi = 10^5$ Hz, and orientational angle $\varphi_h = 0$ at the growth-induced anisotropy constant $K_u = -10^3$ erg cm^{-3} and the magnetizing fields $H = 276.8$ Oe (Fig. 1b) and 277.0 Oe (Fig. 1c). It can be seen that the dynamic jumps are accompanied by rapidly relaxing high-frequency oscillations with the period $T \approx 2\pi/\omega_r$; the hopping period, i.e., the total period of these stationary regimes, corresponds to the period of the ac magnetic field. In the cases considered, the trajectory of the magnetization vector encompasses all the four energy minima. Because $\omega \ll \omega_r$, the parameters of the structure and of the external magnetic fields combine such that the magnetization is 'pushed' to one of the energy minima, and a subsequent variation of the phase of the ac magnetic field $\mathbf{h}$ results in the magnetization passing to another energy minimum, etc. Near the value $H = H_+$, the magnetization trajectory encompasses only two energy minima, hopping between them. For the magnetizing field $H = 277.9 \pm 0.1$ Oe, dynamic hopping between three equilibria (including the normally oriented one) is established.

As a result of the realization of the above dynamic regimes, high amplitudes of the magnetization oscillations, which are mainly determined by the orientations of equilibrium states, can be obtained in a wide range of frequencies. Because the amplitude of such regimes only weakly depends on the amplitude of the ac field, they should be classified as auto-oscillating regimes.

3. Multiturn precession of magnetization in [100] films

The specific features of magnetization reversal in iron–garnet films substantially depend on the orientation of the crystallographic axes [61]. The same can be expected of the

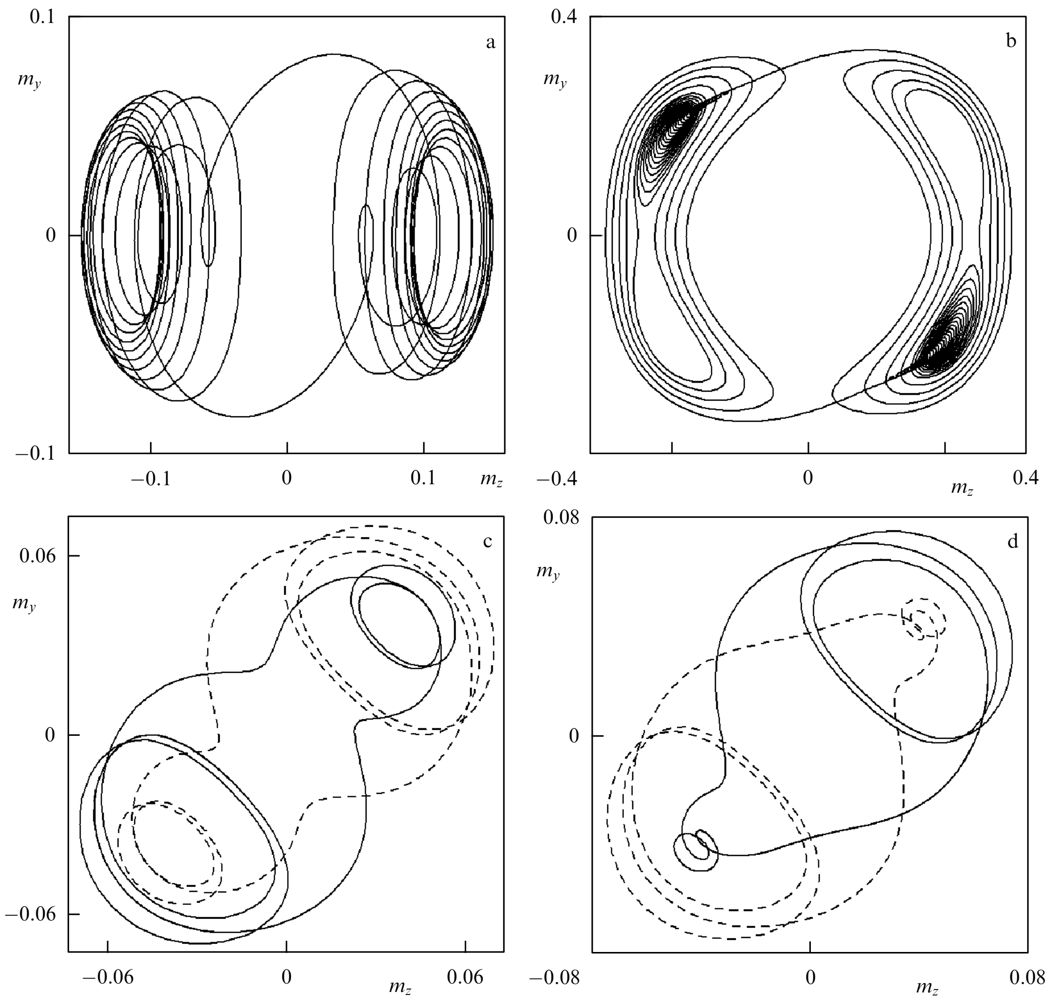

Figure 2. The yz plane projections of stationary orbits of the precession of the magnetization vector at $\omega/(2\pi) = 10^6$ Hz, and $K_1 = -10^3$ erg cm^{-3}: (a) $h = 1$ Oe, $\varphi_h = \pi/2$, $K_u = -10^3$ erg cm^{-3}, and $H = 450$ Oe; (b) $h = 1$ Oe, $\varphi_h = \pi/2$, $K_u = -10^3$ erg cm^{-3}, and $H = 410$ Oe; (c) $h = 0.1$ Oe, $\varphi_h = -\pi/4$, $K_u = -10^3$ erg cm^{-3}, and $H = 450$ Oe; and (d) $h = 0.1$ Oe, $\varphi_h = -\pi/4$, $K_u = 0$, and $H = 332$ Oe.

arising precession regimes. We now consider the dynamics of magnetization in a film of another type.

In the investigations and various practical applications of iron garnets, (100) films are widely used because they allow most easily ensuring the perpendicular orientation of the easy axis to the film plane; this orientation is least sensitive to various inhomogeneities of composition and changes in voltage and temperature [62].

For (100) films, it is assumed that the crystallographic axis [100] coincides with the x axis and is normal to the film surface, and the [010] and [001] axes coincide with the y and z axes. In the case under consideration, the growth-induced anisotropy remains the same as before and the density of the free energy of magnetocrystalline anisotropy is written as

$$F_a = \frac{1}{4} K_1 \left(\sin^2 2\theta + \sin^4 \theta \sin^2 2\varphi \right) . \tag{7}$$

The frequency of the linear resonance in the case of the equilibrium orientation of the vector $\mathbf{M}$ perpendicular to the film surface ($\theta_0 = 0$) is given by

$$\omega_r = \gamma \left[H - 4\pi M + \frac{2(K_u + K_1)}{M} \right] . \tag{8}$$

A characteristic feature of the nonlinear precessional motion of the magnetization vector in [100] iron–garnet films is the appearance of complex multiturn trajectories at sufficiently low frequencies ($\sim 10^6$ Hz) and large amplitudes of the ac magnetic field ($h \sim 0.1-1$ Oe) [63]. Figure 2 displays the results of a numerical solution of Eqns (1) represented by the yz projections of the normalized magnetic moment that passes into a stationary precessional orbit under the effect of a microwave field with the frequency $\omega/2\pi = 10^6$ Hz, amplitudes $h = 1$ Oe (Figs 2a, 2b) and $h = 0.1$ Oe (Figs 2c, d), and orientational angles $\varphi_h = \pi/2$ (Figs 2a, b) and $\varphi_h = -\pi/4$ (Figs 2c, 2d); the magnetocrystalline anisotropy constant is $K_1 = -10^3$ erg cm^{-3}; the growth-induced anisotropy constant is $K_u = -10^3$ erg cm^{-3} (Figs 2a–c) and 0 (Fig. 2d); the magnitudes of the magnetizing field $H = 450$ Oe (Fig. 2a) and 332 Oe (Fig. 2d) correspond to the condition of linear resonance (8); in Fig. 2b, $H = 410$ Oe. At $H = 450$ Oe, there is a single energy minimum corresponding to the orientation of the magnetization along the normal. As follows from Fig. 2a, the trajectory of the precessional motion then becomes elongated in the direction of the microwave-field polarization, two symmetric regions with several turns arise in it, and the magnetization vector jumps from one region into another. The period of the precessional motion is equal to that of the ac field. A decrease in the magnetizing field leads to an increase in the amplitude of the trajectory of motion and subsequently to the concentration of turns around two of the four arising equilibrium directions differing from the normal (Fig. 2b). The turns in this case arise around one of the two pairs of equilibrium positions lying along the diagonal. Thus, a dynamic bistability occurs, i.e., the existence of two trajectories of magnetization precession identical in shape but differently oriented; the realization of one of them can be affected by fluctuations of the various parameters of the system or by the initial phase of the ac magnetic field. These regimes are orientational dynamic jumps and their amplitude is determined by the orientations of equilibrium states. In narrow ranges of the ac-field frequency, stochastic regimes have been revealed characterized by an arbitrary changeover of equilibrium positions between which these jumps occur. A further decrease in the magnetizing field leads to low-amplitude precession regimes corresponding to one of the four equilibrium orientations of the magnetization. With increasing H, the precession amplitude decreases and the trajectory of motion is simplified. With increasing the frequency ω, progressively greater amplitudes of the microwave field are required to obtain the above trajectories of precessional motion; at small h, a virtually linear precession is observed. At large resonance frequencies ($\omega/2\pi \geqslant 10^8$ Hz), the main nonlinear effect is a nutational motion of the magnetization vector with the frequency that is twice the precession frequency (frequency doubling).

In a specific sample with a fixed magnetocrystalline anisotropy, the parameters of the growth-induced anisotropy can be varied using thermal annealing [62]. But in the case under consideration, as was shown in [63], the amplitude of the magnetic moment precession depends to a greater extent on the field of the magnetocrystalline anisotropy than on the growth-induced anisotropy. To increase the precession amplitude, materials with the lowest (in amplitude) anisotropy constant K_1 should be taken. A significant increase in the growth-induced anisotropy decreases the amplitude of the precessional motion of the magnetization vector but does not result in simplifying its trajectory.

At the amplitudes of the microwave field $h \sim 0.1$ Oe and its polarization directions $\varphi_h \neq 0\ \pi/2$, or π, an asymmetry of the precessional motion trajectory is observed (Figs 2c, d), which reaches its maximum at $\varphi_h = \pm\pi/4$. It can be seen that the asymmetry increases with decreasing the growth-induced anisotropy and that a dynamic bistability occurs, i.e., two stationary orbits of the precessional motion symmetric with respect to the x axis exist. The establishment of the stationary motion along a certain orbit can be affected by fluctuations in the various parameters of the dynamic system, in particular, in the initial phase of the microwave field (the solid curves were plotted at the initial phase $\vartheta = 0$ and the dashed curves at $\vartheta = \pi$). In the case of a significant increase or decrease in the amplitude of the field, the asymmetry of the motion trajectory and, correspondingly, the dynamic bistability disappear.

4. Dynamic effects in metallic two-layer structures

4.1 Equilibrium states

We begin the consideration of the multilayer magnetically coupled structures that have been intensely studied in recent years with a system consisting of two metallic layers separated by a nonmagnetic interlayer (spacer). We assume that each of the layers of thickness d_i (where i labels the layers) has a magnetization $\mathbf{M}_i$, an induced uniaxial anisotropy with a constant K_{ui} and an easy axis lying in the film plane (along the y axis), which is characteristic of metallic polycrystalline films. Then, the density of the free energy of the system is written as

$$F = F_1 + F_2 + AM_1M_2d_{12} \times \left(\cos\psi_1\cos\psi_2\cos(\varphi_1-\varphi_2)+\sin\psi_1\sin\psi_2\right), \qquad (9)$$

where each of the terms F_i is determined by Eqn (2), in which the magnetocrystalline anisotropy is neglected and the growth-induced anisotropy is associated with the quantity

$$F_{ui} = K_{ui}\sin^2\varphi_i\,, \qquad (10)$$

which determines the energy of the induced in-plane anisotropy; the third term in the right-hand side of Eqn (9), with a constant A depending in general on the thickness and material of the spacer and on its structural characteristics, describes the coupling between the magnetic layers [64]; $d_{12} = d_1d_2(d_1+d_2)^{-1}$ is the reduced thickness of the two magnetic layers; the azimuthal angle φ_i is referenced to the y axis; and $\psi_i = \pi - \theta_i$ is the angle between the magnetization vector $\mathbf{M}_i$ and the film plane. We assume that the direction of the magnetizing field $\mathbf{H}$ coincides with the easy axis (the y axis). For the chosen geometry of the fields and films with large values of the demagnetizing fields ($4\pi M_i \gg H_{Ki}$, AM_i, where $H_{Ki} = 2K_{ui}/M_i$ is the magnetic-anisotropy field of the ith layer), the equilibrium directions of the magnetization of the layers (at $h = 0$), which are determined by the angles φ_{0i} and ψ_{0i}, lie in the plane of the system; therefore, $\psi_{0i} = 0$. The angles φ_{0i} are determined from the conditions of equilibrium $\partial F/\partial\varphi_i\big|_{\varphi_i=\varphi_{0i}} = 0$ and $\partial^2F/\partial\varphi_i^2\big|_{\varphi_i=\varphi_{0i}} > 0$, which lead to the relations

$$\begin{aligned} &K_i\sin 2\varphi_{0i} + HM_i\sin\varphi_{0i} - D_i\sin(\varphi_{0i}-\varphi_{03-i}) = 0\,,\\ &H_{Ki}\cos 2\varphi_{0i} + H\cos\varphi_{0i} - \frac{D_i\cos(\varphi_{0i}-\varphi_{03-i})}{M_{3-i}} > 0\,, \end{aligned} \qquad (11)$$

where $i = 1, 2$ and $D_i = Ad_{12}M_1M_2/d_i$. In what follows, we consider the case of positive values of the parameter A ($A > 0$), which ensures an antiferromagnetic coupling between the magnetic moments in the layers at $H = 0$, i.e., the case where their directions are opposite (in particular, $\varphi_{01} = 0$ and $\varphi_{02} = \pi$). In a numerical analysis, parameters are used that are close to those of real films of the permalloy class, $H_{K1} = 10$ Oe and $4\pi M_1 = 1.1 \times 10^4$ G for the first film, and $H_{K2} = 5$ Oe and $4\pi M_2 = 8 \times 10^3$ G for the second film; the film thicknesses are assumed to be equal: $d_1 = d_2 = 0.1$ μm.

An analytical solution of Eqn (1) can only be obtained in the case of small equilibrium angles ($\varphi_{0i} \ll 1$), which is the case for $H \gg H_{Ki}$ [65]. But in the general case of the parameters entering Eqn (11), these angles are by no means small; therefore, an analysis of the set of equations (11) can only be performed using numerical methods [66].

Figure 3 shows the equilibrium azimuthal angles between the magnetic moments of two films (obtained for various values of the coupling constant A) as functions of the magnetizing field H oriented in the initial state along the vector $\mathbf{M}_1$. The dashed lines show the limit values of the field H_c corresponding to the disappearance of the equilibrium collinear states with the angles $\varphi_{01} = 0$ and $\varphi_{02} = \pi$. It can be seen that the change in the magnitude of the magnetizing field

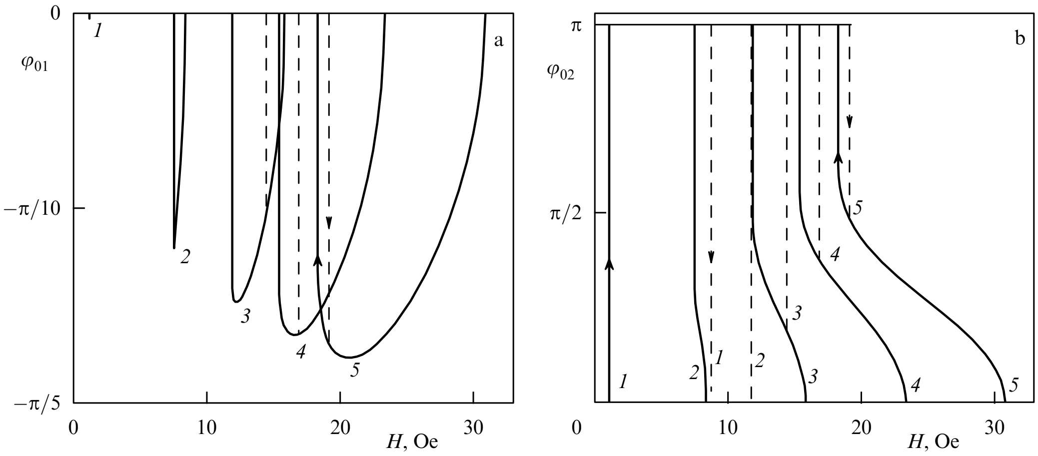

Figure 3. Field dependences of the equilibrium orientations of the magnetic moments of each of the layers on the magnitude of the magnetizing field H for the coupling constants $A = 10^{-2}$, 2×10^{-2}, 3×10^{-2}, 4×10^{-2}, and 5×10^{-2} (curves *1–5*, respectively).

is accompanied in these systems by the appearance of loops of orientational hysteresis (of various shape) and related states of the orientational bistability realized in the range of fields $H_b < H < H_c$. As the magnetizing field increases to H_c, an orientational phase transition in the system of coupled magnetic moments occurs. In the case of small values of the coupling constant ($A \leqslant A_c$, curves *1*, *2* in Fig. 3), the direction of the magnetization of the second film is reversed at the phase transition point, and the vector $\mathbf{M}_2$ becomes parallel to the vector $\mathbf{M}_1$. If $A > A_c$ (curves *3–5*), the magnetization reversal of the second film is different from 180° because of the angular 'repulsion' of magnetic moments, and the vector $\mathbf{M}_1$ also deviates from its initial direction. At $H = H_c$, the state of the system with $\varphi_{02} = \pi$ becomes unstable and the magnetization of the second film, with equal probability, can turn in the direction of either $\varphi_{02} < \pi$ or $\varphi_{02} > \pi$. Correspondingly, the magnetization of the first film rotates in the direction of either $\varphi_{01} < 0$ or $\varphi_{01} > 0$. As a result, one of the two equilibrium states symmetric with respect to the direction of the applied field is established. A further increase in the field leads to a decrease of the angle between $\mathbf{M}_1$ and $\mathbf{M}_2$; this angle vanishes at $H = H_a$, i.e., the equilibrium at $H \geqslant H_a$ is given by the codirectional state of these vectors.

With a decrease in the magnetizing field, in the case of the initial codirectional orientation of magnetic moments, one of the two symmetric noncollinear states is realized after the bifurcational value $H = H_a$ is reached. To the noncollinear states of the magnetic moments of the films, there corresponds an interval of the magnetizing field $H_b < H < H_a$, which increases as the coupling constant increases. At $H = H_b$, an orientational phase transition occurs, leading to a state with oppositely directed magnetic moments of the films. For small values of the coupling constant (curves *1* and *2*), as was already noted, $H_b \approx H_a$; therefore, the noncollinear equilibrium states are virtually absent. Depending on the magnitude of the coupling constant A, the value of H_a can be either greater or lower than H_c. At a chosen direction of the magnetizing field, $H_c > H_b$ and the change in H leads to an orientational hysteresis. It can be seen that as the coupling constant increases, the values of H_c and H_b become closer to each other and, consequently, the hysteresis loop narrows. The width of the hysteresis loop can be reduced to a few fractions of an oersted, which is very important for the realization of the dynamic regimes considered in Section 4.2.

The exact value of the field H_c at which the state with the angles $\varphi_{01} = 0$ and $\varphi_{02} = \pi$ ceases to be equilibrium is determined by the expression

$$H_c = \frac{1}{4}\left(G_1 + \sqrt{G_1^2 + 8G_2}\right), \tag{12}$$

where

$$G_1 = A\,(M_1 - M_2) + 2(H_{K2} - H_{K1})$$

and

$$G_2 = A\,(M_1 H_{K1} + M_2 H_{K2}) + 2H_{K1}H_{K2}\,.$$

The magnitude of the field H_a can be obtained from Eqn (12) by changing the sign of M_2 and H_{K2}. The value of the coupling constant A_c is found from the equality $H_c = H_a$.

The direction reversal of the magnetizing field (to $\alpha = \pi$) leads to an analogous situation: the equilibrium state with the angles $\varphi_{01} = 0$ and $\varphi_{02} = \pi$ vanishes at a field exceeding some critical value and the magnetization of the first film changes its direction, which at sufficiently large A (in the cases under consideration, at $A \geqslant 0.03$) is accompanied by a change in the direction of the magnetization of the second film. The value of this critical field can be found from Eqn (12) with the reversed sign of G_1.

Near the values of the field $\mathbf{H}$ at which the change in the orientation of the magnetization in the layers has a jumplike character, conditions arise that are most favorable for the excitation of various dynamic regimes, which are sensitive to small changes in the parameters of the system and in the magnitudes of the fields, by a weak high-frequency field $\mathbf{h}$.

4.2 Dynamic magnetization reversal in a transverse field h

With switching on a high-frequency field $\mathbf{h}\,(t)$, the expressions for the susceptibility of the system and separate layers in the linear approximation with respect to small deviations from the equilibrium position ($\delta_i = \varphi_i - \varphi_{0i}$ and ψ_i) take the form

$$\chi = \frac{d_1\chi_1 + d_2\chi_2}{d_1 + d_2}\,,$$

$$\chi_i = 4\pi\gamma^2 M_i\,\frac{M_i\Delta_{3-i}\cos\varphi_{0i} - 4\pi\gamma^2 D_i M_{3-i}\cos\varphi_{03-i}}{\Delta_1\Delta_2 - 16\pi^2\gamma^4 D_1 D_2}\,, \tag{13}$$

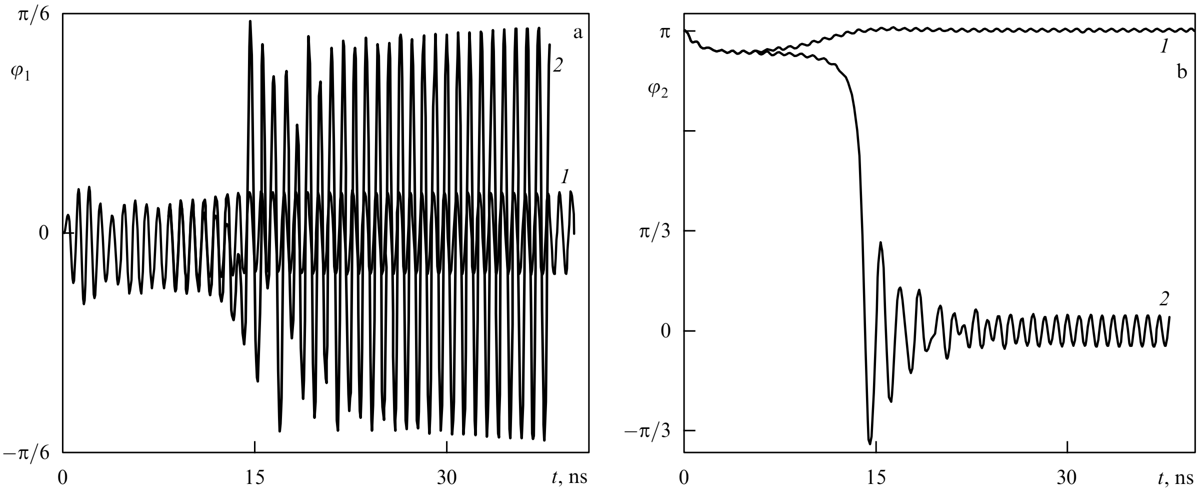

Figure 4. Time dependences of the azimuthal angle of magnetic moments of the first (a) and second (b) films at the frequency $\omega = 7 \times 10^9$ s^{-1} $\approx \omega_{01}$ at two amplitudes of the microwave field close to the critical value: $h = 0.70$ (*1*) and 0.71 Oe (*2*).

where $\Delta_i = \omega_{0i}^2 - \omega^2 - 4\pi\gamma^2 D_i + 4\pi i \lambda_i \omega$, $D_i = A d_{12} M_1 M_2 \times \cos(\varphi_{0i} - \varphi_{03-i})/d_i$, and $\omega_{0i}^2 = 4\pi M_i \gamma^2 (H \cos\varphi_{0i} + H_{Ki} \cos 2\varphi_{0i})$ are the resonance frequencies of the isolated layers.

Near the edges of the hysteresis loop, the system is most sensitive to an external action; therefore, the equations of motion here should be solved numerically. It follows from a numerical analysis of the equations of motion that for a transverse ($\mathbf{h} \perp \mathbf{H}$) linearly polarized (in the film plane) microwave field and the magnetizing field close to the critical value H_c ($H_c - H \leqslant 0.5$ Oe), we can choose the amplitude of the ac field h_c at any frequency ω such that a precession with oppositely directed axes occurs at $h < h_c$, whereas a dynamic magnetization reversal of the system from the initial configuration with the angles $\varphi_{01} = 0$ and $\varphi_{02} = \pi$ occurs at $h > h_c$, and a precessional motion of the magnetic moments of the films with codirectional axes is established [67].

Figure 4 displays time dependences of the azimuthal angle of the magnetic moments of the first (Fig. 4a) and second (Fig. 4b) films going into stationary orbits at the coupling constant $A = 0.01$ and the frequency $\omega = 7 \times 10^9$ s^{-1}, which is close to the resonance frequency of the first film ω_{01} at the microwave field amplitudes $h = 0.70$ and 0.71 Oe (curves *1* and *2*), which were chosen to be lower and greater than the critical value h_c, respectively. The value of the magnetizing field $H = 8.6$ Oe was chosen such that it is close to the critical field H_c for a given value of A and an equilibrium state with the opposite directions of the magnetic moments of films with angles $\varphi_1 = 0$ and $\varphi_2 = \pi$ is realized in the absence of the microwave field. It is seen that at the initial stage, the development of precession occurs in both cases in a virtually identical way. But the existing small difference in the trajectories causes a dramatic change in the dynamics of the magnetic moments of the system and leads to the establishment of different precession regimes. The amplitude of the precessional motion under the effect of dynamic magnetization reversal proves to be several times greater, in spite of an only insignificant increase in the amplitude of the microwave field. A similar situation can be obtained by varying the frequency of the microwave field ω near its critical value at a constant amplitude of h.

For the above values of the coupling constant and magnetizing field, Fig. 5 displays the frequency dependences of the high-frequency susceptibility of the system $\tilde{\chi} = (M_1 \cos\tilde{\varphi}_1 + M_2 \cos\tilde{\varphi}_2)/h$, where $\tilde{\varphi}_i$ are the amplitudes of the azimuthal angles of the stationary oscillations of the magnetic moments of the corresponding layers obtained at various field values $h = 0.1$, 0.2, 0.5, and 1 Oe (curves *1–4*, respectively). The dashed curves correspond to linearized solutions plotted based on Eqn (13) for the equilibrium orientations $\varphi_{01} = \varphi_{02} = 0$ (curve *5*) and $\varphi_{01} = 0$ and $\varphi_{02} = \pi$ (curve *6*). It follows from these dependences that at the frequencies $\omega \leqslant 10^9$ s^{-1}, even at the amplitudes of the microwave field $h \leqslant 0.1$ Oe, a magnetization reversal of the second film of the system occurs, and a precession of the magnetic moments with codirectional axes is established. Beginning with a certain frequency, which depends on the microwave field amplitude, the magnetization reversal is not realized and the precession axes of the magnetic moments of the two films remain oppositely directed. With increasing the field amplitude h, the range of frequencies of the magnetization-reversing field expands into the region of greater values. Thus, this range involves the first resonance region at

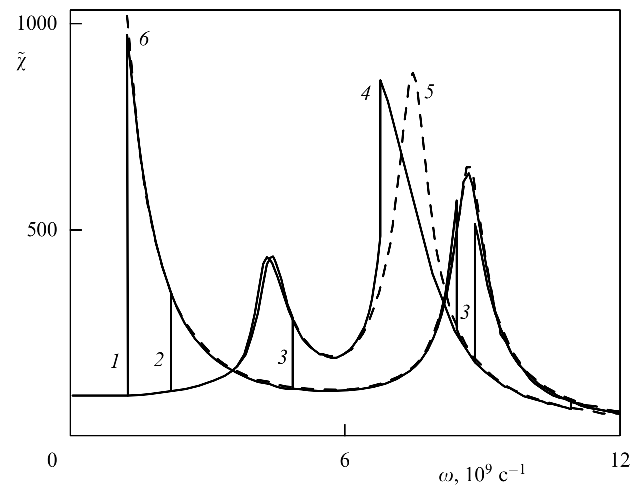

Figure 5. Frequency dependences of the high-frequency susceptibility $\tilde{\chi}$ of the system at various amplitudes of the microwave field. The dashed curves *5* and *6* represent linearized solutions corresponding to $\varphi_{01} = \varphi_{02} = 0$ and $\varphi_{01} = 0$ and $\varphi_{02} = \pi$, respectively.

$h = 0.5$ Oe, and includes both resonance regions at $h = 1$ Oe; the magnetization reversal is absent only at the end of the frequency range under consideration. A characteristic feature of the effect is also the presence of a sufficiently narrow frequency region in which the magnetization reversal occurs bordering the resonance frequency of the system in the initial configuration $\varphi_{01} = 0$ and $\varphi_{02} = \pi$ (curve *3*) and narrowing up to the complete disappearance with decreasing the amplitude of the high-frequency field h.

A change in the magnitude of the magnetizing field H by a few fractions of an oersted strongly affects the frequency intervals of dynamic magnetization reversal. Depending on the chosen frequency interval, the dynamic magnetization reversal can result in either an increase or a decrease in the precession angles with respect to the precession angles with the oppositely directed axes. As follows from the analysis, an increase in the precession amplitude occurs in the frequency interval $\omega_a < \omega < \omega_b$, whose boundary frequencies can be found from the conditions $|\chi(\varphi_{02} = 0)| = |\chi(\varphi_{02} = \pi)|$. For a structure with magnetic layers of equal thickness, in neglecting damping in the spin subsystem, the approximate expressions

$$\omega_a \approx 2\gamma\sqrt{2\pi K_2}\,,$$
$$\omega_b \approx \gamma\sqrt{4\pi M_1\left(H + H_{K1} + \frac{M_2 A}{2}\right)} \qquad (14)$$

are satisfied sufficiently well for the above frequencies; in a rather wide range of parameters, they give frequencies that differ from the calculated values by no more than 1–5%.

The above-considered behavior of a magnetically coupled system is also observed when the magnetizing field is close to the critical value H_b ($H - H_b \leqslant 0.5$ Oe). The initial configuration may then correspond to the angles $\varphi_{01} = \varphi_{02} = 0$ or to a noncollinear direction of the magnetic moments, and the precession after the magnetization reversal has oppositely directed axes.

4.3 Oscillating regimes in the case of a low-frequency transverse field

Large magnetization precession amplitudes (about 50°) have been experimentally obtained in a permalloy film 10 nm thick upon its excitation by a sequence of magnetic field pulses with the repetition period equal to the resonance frequency of the magnetic system [68]. Obtaining large-amplitude precession regimes with larger deviations of the magnetization angle in the system considered is possible by the application of a longitudinal ac field (**h** || **H**) [69]. In this case, to efficiently excite magnetic oscillations, systems should be used in which narrow ($\Delta H \leqslant 1$ Oe) hysteresis loops are realized; the magnitude of the magnetizing field should then lie inside the hysteresis loop or be close to its critical values. In metallic magnetically coupled multilayer systems with the above-mentioned parameters at small frequencies of the longitudinal field, dynamic regimes arise that manifest themselves in a periodic magnetization reversal of the layers composing the structure.

Figure 6 displays the time dependence of the azimuthal angles of the magnetic moments of the layers at the coupling constant $A = 0.05$, various frequencies ω, the microwave field amplitude $h = 1$ Oe, and the magnetizing field $H = 19$ Oe. The amplitude of the magnetization precession in the polar angle is significantly less than the amplitude of the change in the azimuthal angle; thus, in the absence of a magnetizing field, we have $\psi_i \sim h/4\pi M_i$, whereas $\varphi_i \sim h/H_{Ki}$. It is seen from these dependences that at a sufficiently low frequency (Fig. 6a), a 'pulsed' regime of oscillations arises with short transient regions and with the period equal to the ac field period T_h. The amplitude of this regime is determined by the difference in the angles corresponding to equilibrium stationary positions at the chosen magnitudes of H and A

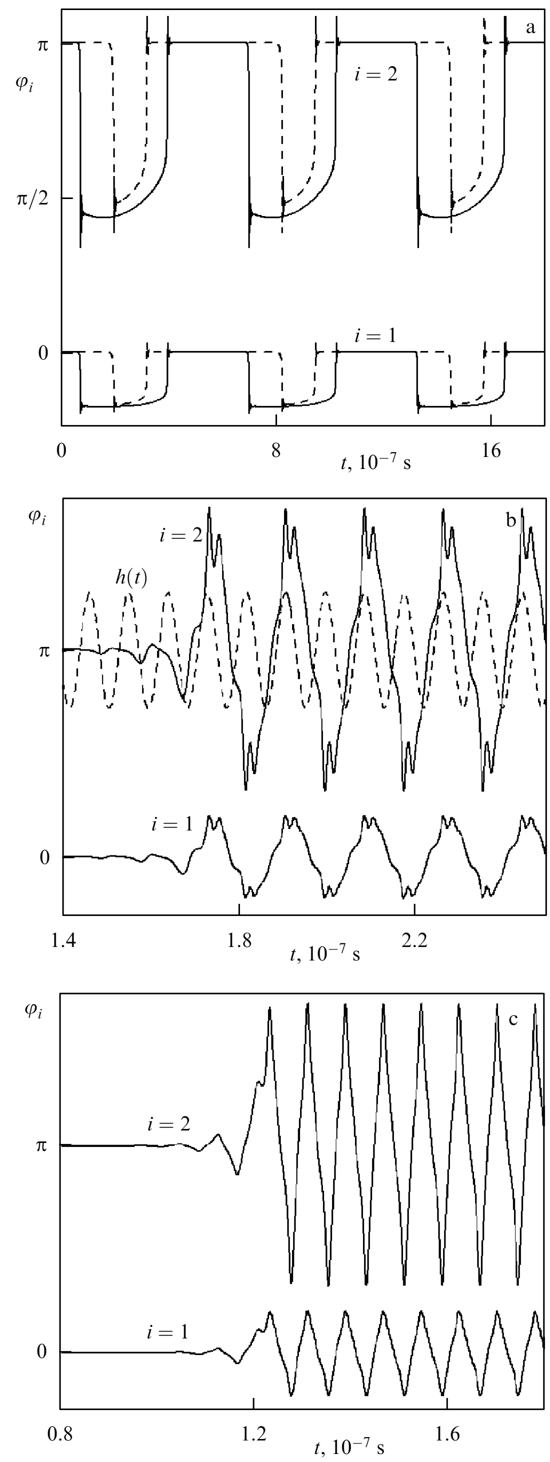

Figure 6. Time dependences of the azimuthal angles of magnetic moments for large-amplitude precession regimes realized at $A = 0.05$, $h = 1$ Oe, and $H = 19$ Oe at various frequencies of the longitudinal disturbing field: $\omega = 0.1 \times 10^8$ s^{-1} (a), $\omega = 7 \times 10^8$ s^{-1} (b), and $\omega = 16 \times 10^8$ s^{-1} (c).

($\varphi_{01} \approx 0, \mp 30°$; $\varphi_{02} \approx 180°, \pm 89°$) and weakly depends on the amplitude of the ac field h. The oscillations of the magnetic moment of each layer occur between two potential wells, and the microwave field withdraws the system from the equilibrium state and compensates the energy losses related to the precessional motion. At $A = 0.05$, the minimum amplitude of the ac field at which a given oscillating regime is realized is equal to $h_{\min} \approx 0.7$ Oe. An increase in h to 1 Oe and to even greater values does not lead to noticeable changes in the parameters of the regime. With an increase in the coupling constant A, the threshold value of the ac field decreases because of the narrowing of the orientational hysteresis loop, and we have $h_{\min} \approx 0.4$ Oe at $A = 0.06$. In this regime, the pulse-period-to-pulse-duration ratio can be controlled by varying the magnitude of the magnetizing field. In particular, as H is shifted to the left-hand side of the hysteresis loop ($H = 18.3$ Oe), the pulse duration decreases, which is shown in the figure by a dashed curve. In this case, apart from the equilibrium orientation with oppositely directed magnetic moments, there are two noncollinear equilibrium orientations, and hence the establishment of two equilibrium regimes of magnetization reversal is possible, with the angles $0 < \varphi_2 < \pi$ and $-\pi < \varphi_2 < 0$. But if a 'pulsed' regime is established, then only one of the above-indicated transitions is realized.

At higher frequencies ($\omega \approx (7-17) \times 10^8$ s^{-1}), large-amplitude oscillating regimes are realized (Figs 6b, 6c) with a doubled period ($2T_h$) and an amplitude that is almost twice the amplitude corresponding to the regime presented in Fig. 6a. In this case, in the given range of frequencies, there exist regions in which large-amplitude chaotic oscillations of magnetic moments occur, as well as a region ($\omega \approx (7.5-8) \times 10^8$ s^{-1}) in which the system is not susceptible to the action of the ac field [69]. The region of dynamic insusceptibility, i.e., the window of transparency of the spin system to the longitudinal microwave field, is preceded by a region of chaotic oscillations, which passes with increasing the frequency into a region of regular oscillations whose amplitude decreases to complete disappearance with increasing the frequency.

In some of their features, the above large-amplitude oscillations are close to the regimes of dynamic orientational jumps of the magnetization vector in iron–garnet films and have much in common for various systems that exhibit bistability. Thus, similar oscillating processes arising under the effect of light were revealed in the system of two thin films with a resonance nonlinearity in [70]. In magnetic bistable systems (including thin-film ones) with random noise, a harmonically varying external field can cause processes of a rapid periodic magnetization reversal of the system with the total period of the dynamic regime equal to the period of the ac field. As the frequency of the external action increases in this case, the magnetization reversal ceases to occur in each period of the ac field, which leads to weak chaotization of this process [71].

5. Bistable states in magnetically coupled metallic sublattices

5.1 Equilibrium states

We now consider single-crystal multilayer structures with a strong interlayer coupling typically caused by the indirect exchange interaction [72]. To exclude the effect of surface layers, we assume that the system studied consists of a sufficiently large number ($n \gg 1$) of layers of a magnetic metal of thickness d_i with a magnetization $\mathbf{M}_i$, which are separated by nonmagnetic spacers whose thickness ensures the antiferromagnetic type of coupling between the magnetic layers. The interfaces between the layers are assumed to be sufficiently smooth and each layer is assumed to be uniformly magnetized. These approximations are widely used in works devoted to orientational phase transitions in multilayer nanostructures [72–74]; their correctness is confirmed by experimental and theoretical investigations of ferromagnetic resonance in structures such as $(\mathrm{Fe/Cr})_n$ [75]. According to the experimental data in [76], the magnetic anisotropy of the magnetic layers in such structures is a combination of the uniaxial induced anisotropy (the type with an easy axis oriented perpendicularly to the layers) and the cubic magnetocrystalline anisotropy (with crystallographic axes [100] and [010] lying in the plane of the layers). The density of the free energy of the system is then given by

$$F = \sum_{i=1}^{n} \left(F_i + \frac{J \boldsymbol{\mu}_i \boldsymbol{\mu}_{i+1}}{2} \right), \tag{15}$$

where $\boldsymbol{\mu}_i = \mathbf{M}_i / M_i$ and J is the constant of bilinear coupling caused by the indirect exchange interaction of the magnetic moments of neighboring layers, which in general depends on the thickness and type of material and on the structural characteristics of the spacer. For each of the magnetic layers, F_i is determined by Eqn (2) with the energies related to the magnetocrystalline and the growth-induced anisotropy described by Eqns (7) and (4). The magnetic layers are assumed to be identical, i.e., it is assumed that $M_i = M$, $d_i = d$, and the constants of the cubic and growth anisotropy are $K_{1i} = K_1$ and $K_{ui} = K_u$. Then, the entire ensemble of magnetic layers can be divided into two subsystems ($j = 1, 2$) with an identical behavior of the layers of each subsystem. The coupling constant J is assumed to be positive, which ensures an antiferromagnetic coupling of the magnetic moments in neighboring layers.

For metallic layers, the magnitude of the demagnetizing field $4\pi M$ is much greater than the field of the growth-induced uniaxial anisotropy $H_K = 2K_u/M$, and hence, in the absence of an external magnetizing field, the magnetic moment of one of the neighboring layers is oriented in the plane of the corresponding layer along the crystallographic direction [100] (to which the azimuthal angle φ_j of the magnetic subsystem is referenced), and the magnetic moments in neighboring layers are directed opposite to this direction. Thus, in the case of an in-plane magnetizing field, the magnetic moments lie in the plane of layers and the equilibrium angles are $\psi_{0j} = 0$. The corresponding azimuthal angles $\varphi_{0j}(H)$ are determined from the equilibrium conditions for the two magnetic systems, which are written as

$$\begin{gathered} 2HM \sin(\varphi_{0j} - \varphi_H) + K_1 \sin 4\varphi_{0j} \\ - 2J \sin(\varphi_{0j} - \varphi_{03-j}) = 0\,, \\ HM \cos(\varphi_{0j} - \varphi_H) \\ + 2K_1 \cos 4\varphi_{0j} - J \cos(\varphi_{0j} - \varphi_{03-j}) > 0\,, \quad j = 1, 2\,, \end{gathered} \tag{16}$$

where φ_H is the angle (referenced to the [100] axis) that determines the in-plane direction of the field $\mathbf{H}$. Then, based on [16], we can investigate the equilibrium states of the magnetizations of the two systems in the case where the magnetizing field is oriented along the direction [100]. In a numerical analysis, parameters close to those characteristic of the $(\mathrm{Fe/Cr})_n$ system are used: the magnetization of iron layers $M = 1260$ G, the anisotropy constants $K_1 = 4.6 \times 10^5$ erg cm^{-3}, $K_2 = 1.5 \times 10^5$ erg cm^{-3}, $K_u = 2.06 \times 10^6$ erg cm^{-3}, the layer thickness $d = 21.2 \times 10^{-8}$ cm, and the damping constant $\lambda = 5 \times 10^7$ s^{-1}; the parameters of the chromium layers do not enter Eqn (15) explicitly, but determine the value of the coupling constant J [77].

Figure 7 shows the dependences of the equilibrium azimuthal angles φ_{01} (solid curves) and φ_2 (dashed curves) of the magnetic moments of two neighboring films on the magnitude of the magnetizing field H obtained for the values of the coupling constant $\bar{J} = 0.1$ erg cm^{-2} (curve *1*) and $\bar{J} = 0.2$ erg cm^{-2} (curve *2*), where $\bar{J} = Jd/2$ [78]. At the initial orientations of the magnetic moments $\varphi_{01} = \pi$ and $\varphi_{02} = 0$, the equilibrium state of the system is the initial one in the range of H from 0 to H_c. When the field reaches H_c, a jumplike orientational phase transition in the entire system occurs. In the case of small coupling constants (curve *1*), the magnetic moments become codirectional: $\varphi_{01} = \varphi_{02} = 0$. In the case of a sufficiently strong interlayer coupling (curve *2*), the magnetization reversal of the films with $j = 1$ proves to differ from 180° because of the antiferromagnetic interaction of neighboring magnetic moments. The angular 'repulsion' of magnetic moments also causes a change in the direction of the magnetization of films with $j = 2$; in this case, we obtain $\varphi_{02}(H_c) = -\varphi_{01}(H_c)$. With a further increase in the field, the angle between the magnetization vectors of neighboring films decreases, and at $H = H_a$, when this angle reaches the minimum value $\varphi_{01} - \varphi_{02} = 2\varphi_a(J)$, which decreases as the coupling constant increases, a second phase transition occurs, which leads to a state with an orientation of the magnetic moments that is codirectional with the field. As the magnetizing field decreases from the magnitude $H > H_a$ at which the initial state is one with a codirectional orientation of the magnetic moments of the films, this state is retained down to the field values $H_b < H_a$. At $H = H_b$, a reverse orientational phase transition occurs, which is accompanied by a jumplike 'divergence' of the vectors $\mathbf{M}_1$ and $\mathbf{M}_2$ to the angles $\varphi_{01}(H_b) = -\varphi_{02}(H_b)$. A further decrease in the magnetizing field leads to a gradual increase in the angle between the magnetizations, which again becomes equal to π at $H = 0$. But none of the magnetic moments separately returns to the initial state.

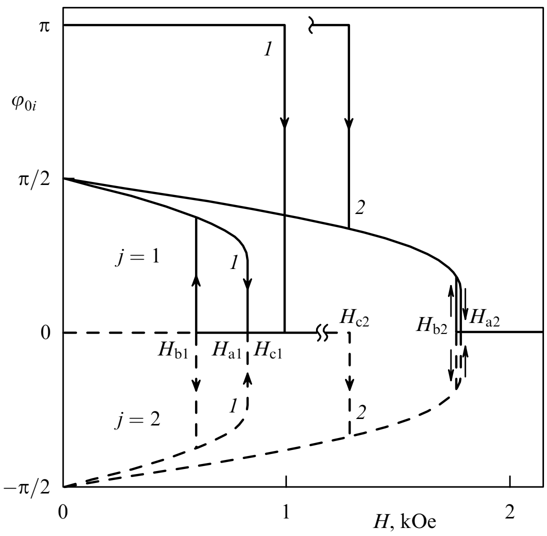

Figure 7. Dependences on the magnetizing field for the equilibrium azimuthal angles φ_{01} (solid lines) and φ_{02} (dashed lines) upon the in-plane 180° and 90° magnetization reversal: $\bar{J} = 0.2$ erg cm^{-2} (*1*) and $\bar{J} = 0.2$ erg cm^{-2} (*2*).

Thus, switching on a magnetizing field of magnitude $H > H_c$ and subsequently switching it off leads to a rotation of magnetic moments through the angle $\pi/2$, i.e., the initial configuration with the angles $\varphi_{01} = \pi$ and $\varphi_{02} = 0$ passes into a configuration with $\varphi_{01} = \pi/2$ and $\varphi_{02} = -\pi/2$. From the energy standpoint, this orientation of magnetic moments is equivalent to the initial orientation, in view of the anisotropy type of magnetic layers and the chosen position of the crystallographic axes. In the case of an in-plane 90° magnetization reversal, which occurs when we have $\varphi_{01} = -\varphi_{02} = \pi/2$ and $\varphi_H = 0$ in the initial state, an increase in the field to a value H_a leads to a gradual convergence of the magnetic moments. At $H = H_a$, as in the above case, an orientational phase transition occurs; as a result, the only equilibrium orientation becomes the codirectional orientation of magnetic moments. The noncollinear configuration is restored upon a decrease in the magnetizing field as a result of the reverse phase transition when the field reaches H_b. Thus, an orientational hysteresis loop arises, which narrows with increasing the coupling constant. But in the case of large coupling constants, $H_b = H_a$ and the hysteresis loop is absent.

The exact expressions for the critical values of the fields, which can be obtained from the set of equations for the equilibrium angles, are given by

$$H_a = \frac{4}{3M}\sqrt{\frac{J + K_1}{6K_1}}(J + K_1)\,, \quad H_b = \frac{2}{M}(J - K_1)\,,$$
$$H_c = \frac{2}{M}\sqrt{K_1(J + K_1)}\,. \tag{17}$$

The minimum angle between the magnetic moments in the case of their noncollinear configuration is determined by

$$\cos\varphi_a = \sqrt{\frac{J + K_1}{6K_1}}\,. \tag{18}$$

With an increase in the coupling constant, the hysteresis loop narrows; the angle φ_a decreases, and at the value $\bar{J} = \bar{J}_{ab} \approx 0.24$ erg cm^{-2} corresponding to the equality $H_a = H_b$, φ_a vanishes together with the disappearance of the hysteresis loop.

The equilibrium orientations of the magnetic moments at another direction of the magnetizing field were considered in [79, 80]. It was shown in [80], in particular, that when the magnetizing field is oriented along the crystallographic axis [110], i.e., at $\varphi_H = \pi/4$, the magnetization reversal is accompanied by a bifurcation: as the magnetizing field becomes less than the bifurcation value $H_b^{(\pi/4)}$, the magnetization reversal in the system of coupled magnetic moments can result in the establishment of equilibrium angles close to either the [100] or the [010] direction. The choice of the direction of the magnetization reversal that occurs as a result of the phase transition is affected by various fluctuations of its parameters, as well as by the parameters that determine the character of the decrease in the magnitude of the magnetizing field.

5.2 Dynamic bistability

Near the critical values of the magnetizing fields corresponding to orientational phase transitions, the system with the antiferromagnetic-type coupling is most sensitive to the effect of a high-frequency field. In the system with a cubic magnetocrystalline anisotropy considered here, a special combination of structure parameters becomes possible such that at $J \approx J_{\rm ca}$, two critical values of the field, $H_{\rm c}$ and $H_{\rm a}$, are close in magnitude [45]. The critical value of the coupling constant at which $H_{\rm c} = H_{\rm a}$ is given by

$$J_{\rm ca} = \frac{3\sqrt{6}-2}{2}\, K_1 \,. \tag{19}$$

Figure 8 displays (for the coupling constant $\bar{J} = 0.132$ erg cm^{-2} close to the critical value $\bar{J}_{\rm ca} \equiv J_{\rm ca}d/2 \approx 0.131$ erg cm^{-2}) the frequency dependence of the high-frequency susceptibility of the system

$$\tilde{\chi} = \frac{M_1 \cos\varphi_{1\rm m} + M_2 \cos\varphi_{2\rm m}}{h} \,,$$

where $\varphi_{j\rm m}$ are the amplitudes of the azimuthal angles of stationary oscillations of the magnetic moments of corresponding layers. The above dependences were obtained for the microwave field amplitudes $h = 0.2$ Oe (Fig. 8a) and 0.4 Oe (Fig. 8b) and for the magnitude of the magnetizing field $H = 1093.2$ Oe, which is close to the critical values $H_{\rm c} \approx 1093.4$ Oe and $H_{\rm a} \approx 1103.2$ Oe. With these parameters of the structure in the absence of the microwave field, an equilibrium state with an opposite direction of the magnetic moments of the films with $\varphi_{01} = 0$ and $\varphi_{02} = \pi$ is realized. The dashed curves in Fig. 8a correspond to the linearized solutions for the high-frequency susceptibility of the system $\chi = \chi_1 + \chi_2$, where

$$\chi_j = \frac{M^2}{\varDelta_1 \varDelta_2 - D^2}\left(D\cos\varphi_{03-j} - \varDelta_{3-j}\cos\varphi_{0j}\right), \tag{20}$$

$$\varDelta_j = \frac{\omega_{0j}^2 - \omega^2 + 4\pi i\lambda\omega}{4\pi\gamma^2} - D\,,$$

$$\omega_{0j}^2 = 4\pi\gamma^2\big(HM\cos(\varphi_{0j}-\varphi_H) + 2K_1\cos 4\varphi_{0j}\big)\,,$$

with $D = J\cos(\varphi_{01}-\varphi_{02})$, plotted for the equilibrium orientations $\varphi_{01} = \varphi_{02} = 0$ (curve *1*), $\varphi_{01} = \pi$ and $\varphi_{02} = 0$ (curve *2*), and a symmetric noncollinear configuration (curve *3*). It can be seen from these dependences that at frequencies not exceeding a certain value $\omega_{\rm c}$, the precession of the magnetic moments with initial oppositely oriented axes is unstable, which leads to a dynamic magnetization reversal of the system. As a result, a precession arises either with codirectional axes or with axes oriented at an angle to one another in accordance with the noncollinear configuration of the magnetic moments of the films corresponding to a given magnetizing field. A dynamic bistability is thus realized at $\omega < \omega_{\rm c}$. Which of the two configurations of the precession axes is realized upon exiting the initial antiferromagnetic phase depends on various fluctuations of the film parameters and magnetic fields, e.g., the initial phase of the microwave field.

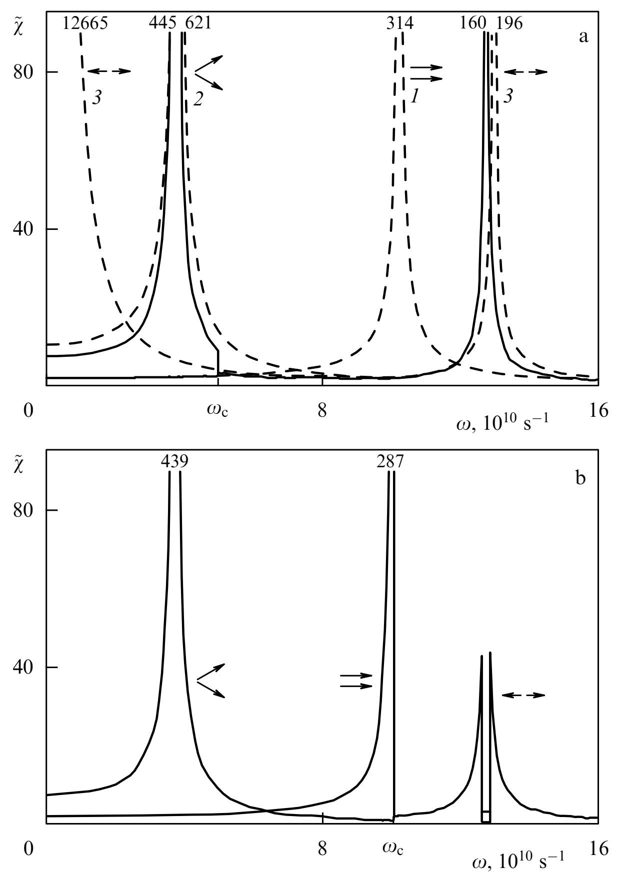

Figure 8. Frequency dependences of the high-frequency susceptibility φ of the system at $\bar{J} = 0.132$ erg cm^{-2}, $H = 1093.2$ Oe, and $h = 0.2$ (a) and $h = 0.4$ Oe (b).

The frequency range of dynamic bistability can easily be controlled because $\omega_{\rm c}$ strongly depends on the microwave field amplitude. An increase in h leads to an increase in the frequency $\omega_{\rm c}$ and an expansion of the dynamic bistability region toward higher frequencies. Thus, at $h = 0.2$ Oe (Fig. 8a), the dynamic bistability region involves only the resonance corresponding to the precession about symmetric noncollinearly oriented axes; at $h = 0.4$ Oe (Fig. 8b), the critical frequency is close to the resonance frequency of the precessional motion of the magnetic moments about codirectional axes; at $h = 1$ Oe (not presented in the figure), the dynamic bistability region completely involves the resonance with both noncollinear and codirectional axes.

At $\omega > \omega_{\rm c}$, no dynamic magnetization reversal is observed in the system and the precessional motion is established around oppositely directed axes. However, at a sufficiently large amplitude of the microwave field (but such that $\omega_{\rm c}$ is less than the frequency of the antiferromagnetic resonance $\omega_{\rm ar}$), a characteristic feature of the dependences considered is the existence of a narrow frequency region near $\omega_{\rm ar}$ (Fig. 8b), where a dynamic magnetization reversal into one of two orientational states of the dynamic bistability occurs. At even greater h, the dynamic magnetization reversal is absent only in the postresonance (with respect to the antiferromagnetic precession with the angles $\varphi_{01} = \pi$ and $\varphi_{02} = 0$) frequency region.

We note that no magnetization reversal is observed in the frequency region preceding the resonance region (for the antiferromagnetic precession) at the initial phase of the microwave field close to $\pi/2$; moreover, the system is virtually unsusceptible to the effect of an ac field. This state is stable with respect to small variations in the initial position of the magnetic moments of the films ($\varphi_{01} = 180 \pm 1°$,

$\varphi_{02} = \pm 1°$) and the phase of the microwave field ($\zeta = 90 \pm 5°$).

The frequency ω_c also strongly depends on the magnitude of the magnetizing field. As H moves away from the critical value H_c, the frequency ω_c decreases. Thus, at $H = 1093$ Oe and $h = 1$ Oe, the dynamic bistability region does not reach the region of resonance with parallel precession axes, completely involving only the resonance of the precessional motion with noncollinear axes. In this case, near the resonance with oppositely directed axes, there is a frequency region of dynamic bistability, which is several times narrower than the corresponding region in Fig. 8b. From the standpoint of the realization of the dynamic bistability state, the approach of the magnetizing field magnitude to the critical value H_c is equivalent to an increase in the microwave field amplitude. The character of the dependence of the high-frequency susceptibility of the system on the magnetizing field magnitude and the presence of a dynamic bistability region are also determined by the microwave field frequency and by the relation between the critical fields H_c and H_a and, consequently, by the value of the exchange coupling constant [45].

The processes of dynamic magnetization reversal in metallic nanostructures caused by the action of a spin-polarized current have been considered, e.g., in [81, 82]. In [81], the auto-oscillations of the magnetization and the dynamic magnetization reversal in the ferromagnetic layer of a magnetically coupled three-layer structure under the action of a spin-polarized electric current passing perpendicularly to the plane of layers were investigated analytically; regimes of dynamic magnetization reversal with various resulting precession amplitudes realized at various values of a current-dependent function have been obtained. In [82], results of experimental investigations of the current-induced magnetization reversal with the development of hysteresis loops in a separate ferromagnetic layer of an asymmetric Cu/Co/Cu system are given; the obtained phase diagrams of the induced dynamics of the magnetization are presented. The experimental data on the current-induced magnetization reversal and oscillations of magnetization alternating in time and corresponding to two different dynamic regimes in multilayer structures of the Co/Cu type have been considered in [83].

6. Asymmetric oscillatory modes in structures with a weak indirect exchange interaction

The noncollinearity of the equilibrium ordering of magnetic moments of neighboring layers allows using a weak in-plane microwave field to excite 'acoustic' and 'optical' oscillating modes [75, 79, 84] corresponding to two normal types of oscillations of a multilayer structure. For the practical use of such structures, an efficient control of the precession regimes and the realization of structurally nonuniform precession regimes are important [75, 85].

The normal modes of the resonance precession of a structure with two magnetic subsystems are associated with the values of the high-frequency magnetic susceptibility χ with the oscillation phase difference of the magnetic moments of neighboring layers $\alpha = 0$ and π. The zero phase difference, i.e., the in-phase oscillations of the magnetic moments of both subsystems, corresponds to the 'acoustic' normal mode excited by the transverse component of the in-plane high-frequency field $h_\perp = h \sin \varphi_h$, where φ_h is the angle that determines the orientation of the field $\mathbf{h}$. The antiphase character of oscillations ($\alpha = \pi$) corresponds to the 'optical' mode excited by the longitudinal field component $h_\| = h \cos \varphi_h$. The positions of maxima in the frequency dependence of the magnetic susceptibility modulus of a multilayer structure $|\chi|$ at fixed values of the magnetizing field correspond to the resonance branches of the $\omega(H)$ dependence. Taking this into account, we can write the magnetic susceptibilities of the system for the acoustic and optical modes as [85]

$$\chi_a = \frac{2M^2 \cos \varphi_0}{\Delta - D}\,, \quad \chi_o = \frac{2M^2 \sin \varphi_0}{\Delta + D}\,, \tag{21}$$

where the parameters Δ and D are analogous to the corresponding parameters in system (20) because $\varphi_0 = \varphi_{01} = -\varphi_{02}$ is the azimuthal angle (we consider the case where the orientational angle of the magnetizing field is $\varphi_H = 0$, and the equilibrium angles are $\varphi_{0j} = \pm \pi/2$ at $H = 0$). Here, we assume that $\varphi_h = \pi/2$ for the susceptibility of the acoustic mode χ_a, and $\varphi_h = 0$ for the susceptibility of the optical mode χ_o.

Using the conditions for the maximum of the imaginary part of the magnetic susceptibility of the system ($\partial \chi''_{a,o}/\partial\omega = 0$ and $\partial^2 \chi''_{a,o}/\partial^2\omega < 0$) in the case of a noncollinear orientation of the magnetic moments, we express the resonance frequencies of the acoustic and optical normal modes of the structure as

$$\omega^2_{a,o} = \omega_0^2 \left(V + 2\sqrt{V^2 + 48\pi^4 \lambda^4 \omega_0^{-4}} \right), \tag{22}$$

where $3V = 1 + \pi\omega_0^{-2}(3\pi\lambda^2 - pD\gamma^2)$ and $p = 0$ for the acoustic and optical modes. It follows from these expressions that the acoustic mode frequency is affected by the exchange interaction only through the equilibrium angles of the magnetic moments. In the case of saturation, a codirectional orientation of the magnetic moments of the subsystems along the magnetizing field ($\varphi_0 = 0$), and a uniform microwave field, the spectrum contains only the acoustic mode and the related frequencies are independent of the magnitude of the interlayer exchange interaction. The case of a nonuniform ac field was considered in [75]; the multiphase character of the resonance precession in layered structures was considered in [86].

The value of the magnetizing field H_{int} corresponding to the intersection of the branches of the two modes is determined from the solution of the equation $\omega_a = \omega_o$. A numerical analysis shows that with increasing the coupling constant, the H_{int} field monotonically increases and that its dependence on the parameter J is nearly linear. The high-frequency magnetic susceptibilities $\chi_{a,o}$ of the system obtained from Eqns (21) monotonically decrease with increasing the coupling constants. Therefore, to obtain greater amplitudes of the precession of the magnetic subsystems, structures with lower values of the exchange interaction constant should be taken.

When the high-frequency field is oriented at an angle $\varphi_h \neq 0, \pi/2$, both oscillating modes are excited, but only one of them can be in resonance (either the acoustic or the optical mode). An exception is the case where the values of the parameters of the system and applied magnetic fields are sufficiently close to those at which the corresponding resonance branches intersect. A similar situation is characteristic of two-sublattice antiferromagnets; when the orientation of the magnetizing field lies in the easy plane, no 'repulsion' of the two branches of the antiferromagnetic resonance is observed, and a frequency-related degeneracy of the two precession modes occurs at the point of their intersection [24].

Based on a numerical solution of the dynamic equations, we now consider the regimes of the precession of magnetic moments of both subsystems in the region of the intersection of the optical and acoustic resonance branches $\omega(H)$. To decrease the indirect exchange coupling, a trilayer structure of the 'sandwich' type can be used instead of multilayer structures [72, 75]. In this case, the quantities J in Eqns (15)–(18) and (20) must be replaced by $J_s = J/2$. The other parameters of the Fe/Cr/Fe structure are assumed to remain unaltered.

For the coupling constant $\bar{J}_s = 0.4$ erg cm^{-2} (where $\bar{J}_s = J_s d$), Fig. 9 shows the variation of the precession amplitude $\delta_{im} = \varphi_i(t)_{max} - \varphi_i(t)_{min}$ ($i = 1, 2$ labels the magnetic layer) of the magnetic moments $\mathbf{M}_1$ (solid curves) and $\mathbf{M}_2$ (dashed curves) as functions of the microwave field orientation at $\omega = 5.9 \times 10^{10}$ s^{-1}, the microwave field amplitude $h = 1$ Oe, and $H = 1625$, 1628, 1633, 1634, 1635, and 1639 Oe (curves *1–6*, respectively). It can be seen from the figure that near the magnetizing field and the ac field frequency values corresponding to the intersection of the optical and acoustic branches, a substantial difference in the amplitudes φ_h and δ_{1m} and δ_{2m} can be obtained by adjusting the in-plane angle φ_h. However, the $\delta_{im}(\varphi_h)$ dependence has a different type at some values of H: when the orientational angle of the ac field reaches a certain critical value, a phase transition occurs leading to an abrupt change in the magnetic susceptibility of the system; this change is different in each of the layers (curve *5*). It is also important that the transition from one type of the $\delta_{im}(\varphi_h)$ dependence to another (see curves *4* and *5*), which occurs upon a change in H, is also a phase transition.

Curve *5* in Fig. 9 was calculated in the case of a unidirectional variation (in particular, increase) of the angle φ_h. But in this situation, because of the development of a dynamic bistability of the system, a dynamic hysteresis appears: upon a reverse variation (decrease) of φ_h, the phase transition occurs at a different, somewhat smaller value of the angle. A similar dynamic hysteresis is also observed in the case of a change in the magnetizing field at certain values of the orientational angle φ_h of the microwave field.

Figure 10 shows the variation of the precession angles of the magnetic moments $\mathbf{M}_1$ (Figs 10a, c) and $\mathbf{M}_2$ (Figs 10b, d) as functions of the magnetizing field $\mathbf{H}(t)$ slowly changing as $H = H_{01} \pm H_{02}(1 - t/\tau)$, where $H_{01} = 1633$ Oe, $H_{02} = 5$ Oe, and $\tau = 40$ ns. The dependences shown in Figs 10a and 10b correspond to a decreasing field H, and those shown in Figs 10c and 10d to an increasing field H. The parameters used are as follows: the coupling constant $\bar{J}_s = 0.4$ erg cm^{-2}; the amplitude of the microwave field $h = 1$ Oe; its frequency $\omega = 5.9 \times 10^{10}$ s^{-1}; and its direction $\varphi_h = 35°$. It can be seen from Fig. 10 that the precession amplitudes of the two magnetic moments are different and that the difference in these amplitudes at the given parameters can strongly depend on the direction of the change in the magnitude of the magnetizing field, i.e., on the previous state of the magnetic system. The width of the hysteresis loop in this case is sufficiently small ($\Delta H \approx 5$ Oe), which can be used to obtain complex precession regimes by applying an additional longitudinal (with respect to $\mathbf{H}$) ac field.

A significant change in the field H (see curves *1* and *6* in Fig. 9) leads to a convergence of the $\delta_{im}(\varphi_h)$ dependences corresponding to various magnetic layers. A similar effect arises upon deviation of the frequency from the value corresponding to the intersection of the resonance branches. Thus, at the frequencies $\omega = 5.7 \times 10^{10}$ and 6.2×10^{10} s^{-1}, a different character of the dependence of the precession amplitude of the two magnetic moments on the orientation of the microwave field is still retained, but the maximum difference between δ_{1m} and δ_{2m} turns out to be small.

Along with the above-considered asymmetric modes corresponding to the region of intersection of the acoustic and optical branches, precession regimes of a beating type are realized. Figure 11 displays (for the coupling constant $\bar{J}_s = 0.4$ erg cm^{-2}, the magnetizing field $H = 1628$ Oe, and the amplitude and frequency of the microwave field $h = 1$ Oe and $\omega = 6.05 \times 10^{10}$ s^{-1}) dot diagrams in which each dot corresponds to a difference δ_{im} between the neighboring

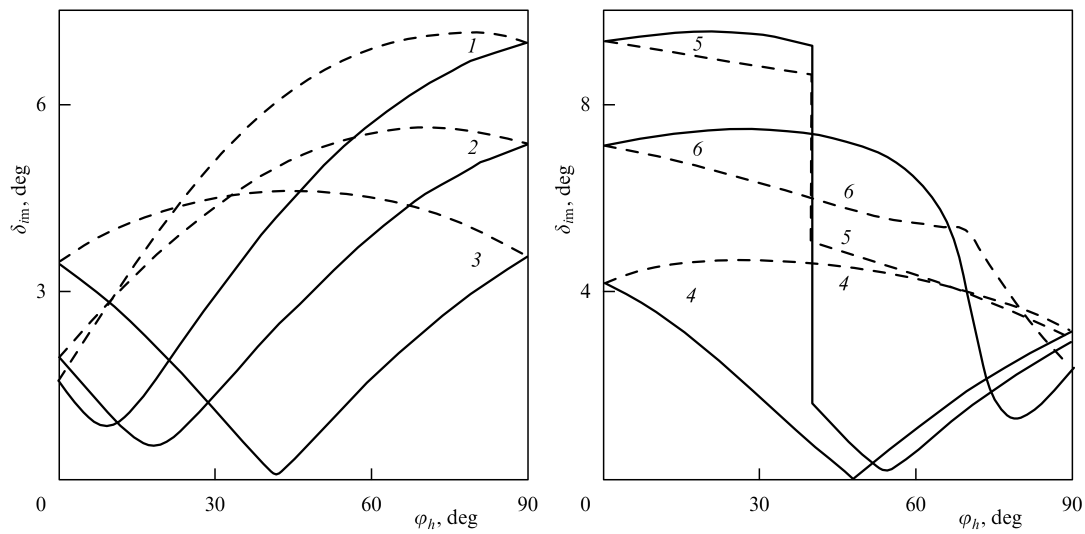

Figure 9. Dependences of the precession amplitude δ_{im} of the magnetic moments $\mathbf{M}_1$ (solid curves) and $\mathbf{M}_2$ (dashed curves) on the orientations of the microwave field at $H = 1625$, 1628, 1633, 1634, 1635, and 1639 Oe (curves *1–6*, respectively), $\omega = 5.9 \times 10^{10}$ s^{-1}, $h = 1$ Oe, and $J = 0.4$ erg cm^{-2}.

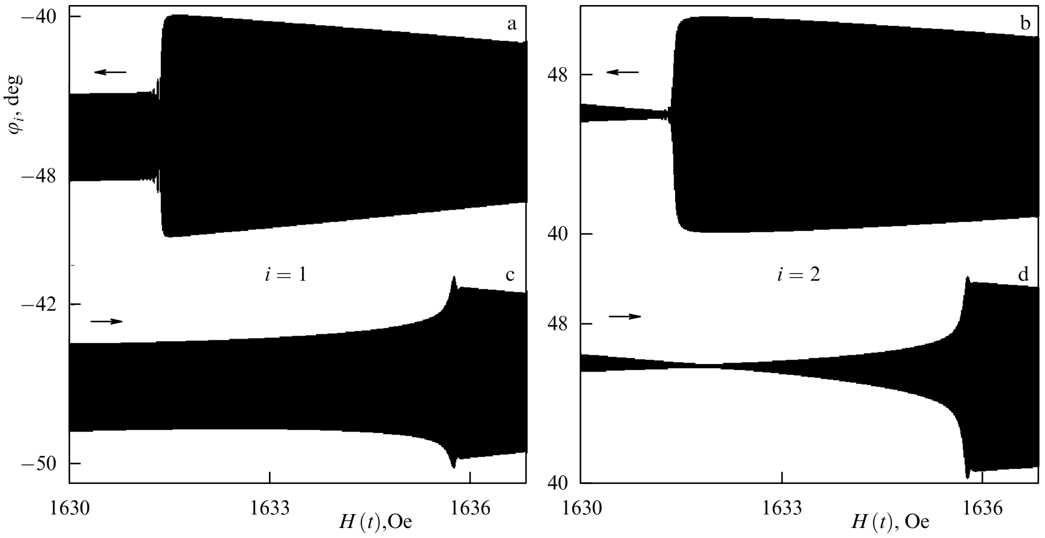

Figure 10. Dependence of the precession angles of the magnetic moments $\mathbf{M}_1$ (a, c) and $\mathbf{M}_2$ (b, d) on the field $\mathbf{H}(t)$ varying as $H = H_{01} \pm H_{02}(1 - t/\tau)$, where $H_{01} = 1633$ Oe, $H_{02} = 5$ Oe, $\bar{J}_s = 0.4$ erg cm^{-2}, $h = 1$ Oe, $\omega = 5.9 \times 10^{10}$ s^{-1}, and $\varphi_h = 35°$.

maximum $\varphi_i(t)_{\max}$ and minimum $\varphi_i(t)_{\min}$ values of the precession of magnetic moments $\mathbf{M}_i$ at a given orientational angle of the microwave field. It can be seen from these diagrams that at the chosen parameters, there are two intervals of the angle φ_h corresponding to regimes in which the amplitude of the precession of magnetic moments not only is asymmetric with respect to the different layers of the structure but also varies in time. The greater density of dots in these intervals indicates that the precession amplitude changes sufficiently smoothly and that the period of this change is very large compared with the period of the microwave field.

Figure 12 displays the time dependence of the precession of both magnetic moments (for the angles $\varphi_h = 32°$, $39.2°$, and $42°$ and for the parameters corresponding to the above diagrams). The value of the orientational angle $\varphi_h = 32°$ falls into the first of the above-mentioned intervals; the value $\varphi_h = 42°$ belongs to the second interval. In the case shown in Fig. 12a, a precession with small beating amplitudes is realized, with the beating period two orders of magnitude greater than that of the microwave field ($T \approx 130 T_h$). The dynamics of one of the magnetic moments in this case only weakly differs from the dynamics of the other. In the case shown in Fig. 12c, the amplitudes of the arising beatings are close to the maximum precession amplitudes and their period increases more than twofold ($T \approx 270 T_h$); in this case, the beatings of the different magnetic moments strongly differ in shape. Between the intervals of the angle φ_h corresponding to the development of beatings, there exists an interval corresponding to asymmetric precession regimes, which are characterized by precession amplitudes that are different for the different magnetic moments but are stationary, i.e., do not vary in time (Fig. 12b). We note that in all the cases where asymmetric modes are realized, the difference between the phases of the first and second magnetic moments is intermediate between 0 and π.

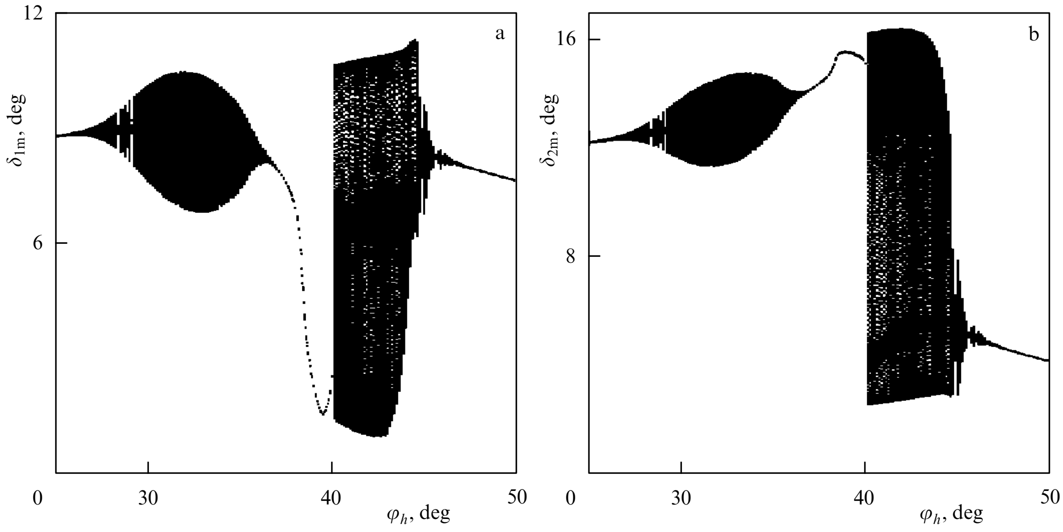

Figure 11. Diagrams of the microwave-field-orientation dependences of the differences δ_{im} between the maxima $\varphi_i(t)_{\max}$ and the corresponding nearest minima $\varphi_i(t)_{\min}$ of the precession of the magnetic moments $\mathbf{M}_1$ (a) and $\mathbf{M}_2$ (b) passing to a stationary regime at $H = 1628$ Oe, $\omega = 6.05 \times 10^{10}$ s^{-1}, $h = 1$ Oe, and $\bar{J}_s = 0.4$ erg cm^{-2}.

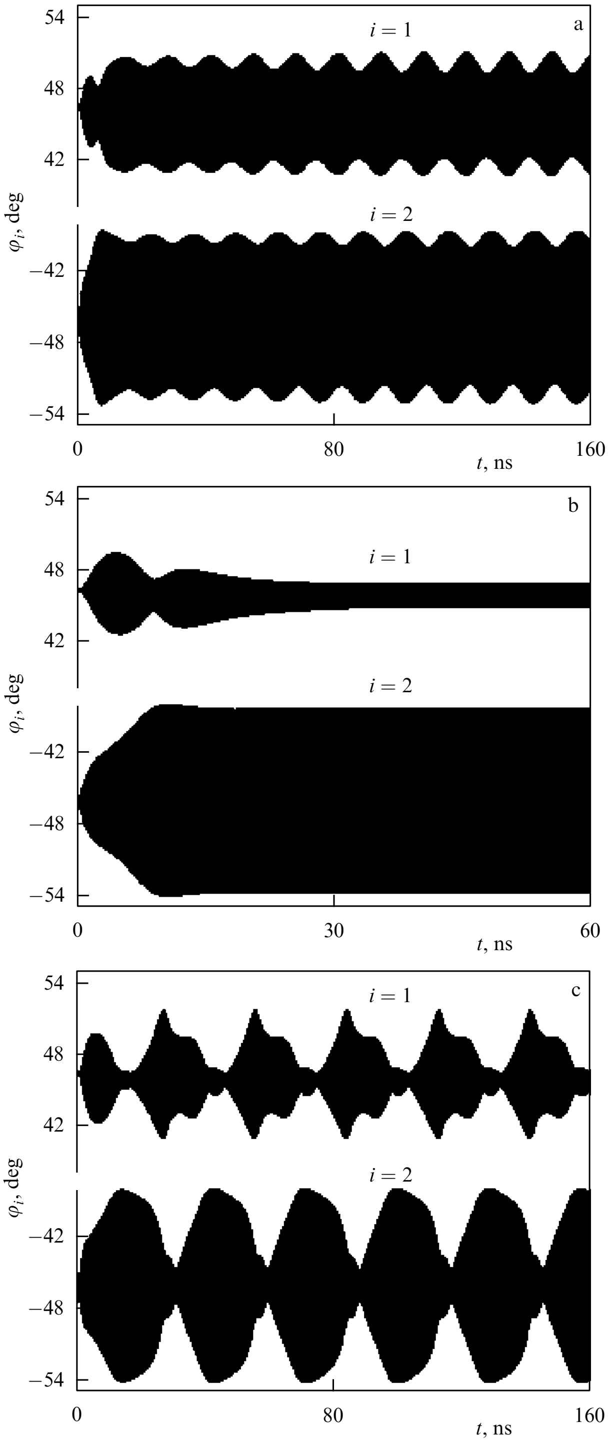

Figure 12. Time dependence of the precession of the magnetic moments of the structure for the orientational angles $\varphi_h = 32°$ (a), $\varphi_h = 39.2°$ (b), and $\varphi_h = 42°$ (c) at $H = 1628$ Oe, $\omega = 6.05 \times 10^{10}$ s^{-1}, $h = 1$ Oe, and $J_s = 0.4$ erg cm^{-2}.

The above results are generally also valid for the structures in which the biquadratic exchange coupling is substantial, along with a bilinear indirect exchange coupling between the magnetic moments of the layers [87]. The density of the free energy of the system is then given by

$$F = \sum_{i=1}^{n} \left[F_i + \boldsymbol{\mu}_i \boldsymbol{\mu}_{i+1} (J_1 + J_2 \boldsymbol{\mu}_i \boldsymbol{\mu}_{i+1}) \right] , \tag{23}$$

where J_1 and J_2 are the constants of the respective bilinear and biquadratic coupling caused by the indirect interaction of neighboring magnetic moments. The equilibrium orientation of the magnetic moments is determined by the set of equations

$$\begin{gathered}
2HM \sin(\varphi_{0j} - \varphi_H) + K_1 \sin 4\varphi_{0j} \\
- 2J_1 \sin(\varphi_{0j} - \varphi_{03-j}) - 2J_2 \sin 2(\varphi_{0j} - \varphi_{03-j}) = 0 , \\
HM \cos(\varphi_{0j} - \varphi_H) + 2K_1 \cos 4\varphi_{0j} \\
- J_1 \cos(\varphi_{0j} - \varphi_{03-j}) - 2J_2 \cos 2(\varphi_{0j} - \varphi_{03-j}) > 0 .
\end{gathered} \tag{24}$$

In the case of the development of a biquadratic coupling, the parameter D in Eqns (20) and (21) takes the form

$$D = J_1 \cos(\varphi_{01} - \varphi_{02}) + 2J_2 \cos 2(\varphi_{01} - \varphi_{02}) . \tag{25}$$

The nature of the biquadratic exchange coupling, the methods of measurements of the constants, and the observed relation have been discussed in [72, 88, 89]. In [53, 89], an explanation of the biquadratic coupling effect, i.e., of a noncollinear magnetic ordering in metallic sublattices, was suggested based on the mechanism of the formation of a short-range antiferromagnetic order with a spin-density wave in chromium near the Fe–Cr interface.

7. Amplitude bifurcations and dynamic bistability in iron–garnet films

The resonance values of the ac field frequency and of the applied dc magnetic field magnitude corresponding to the maximum amplitude of the excited oscillations of magnetization in the films under consideration are adequate notions only for sufficiently small amplitudes and large frequencies of the ac field. For low frequencies of the microwave range, the nonlinear character of the precession motion leads to the appearance of a resonance region of the system parameters in which, along with the well-known effects of frequency doubling and detection, bifurcations of various types are realized, which lead to a change in the dynamic regimes and to the development of dynamic bistability. The most characteristic of these are the above-considered regimes (see Sections 2 and 3) related to orientational jumps from some equilibrium orientations to others under the effect of an ac magnetic field, as well as large-amplitude stochastic and regular regimes caused by the existence of bistable states.

Figure 13 demonstrates bifurcation diagrams for (111) films (Fig. 13a) and (100) films (Fig. 13b) in the plane ($m_{y\mathrm{m}}$, ω), where each of the chosen frequency values of the ac magnetic field corresponds to an extremal value of the y component of the normalized magnetic moment ($m_{y\,\max}$ and $m_{y\,\min}$) precessing in a stationary regime at the ac field amplitude $h = 1$ Oe, the orientational angle $\varphi_h = 0$, the growth-induced anisotropy constant $K_{\mathrm{u}} = -10^3$ erg cm^{-3}, and magnetizing field magnitudes $H = 277$ Oe (Fig. 13a) and 390 Oe (Fig. 13b); the magnetocrystalline anisotropy constant is hereinafter assumed to be $K_1 = -10^3$ erg cm^{-3}. In these diagrams, bifurcations are seen to lead to changes in both the amplitudes of motion (including sharp changes) and the shape of the magnetization precession trajectory. In the region of large-amplitude dynamic regimes, the precession amplitude is mainly determined by the equilibrium orientations of the magnetization; in a sufficiently wide range of the

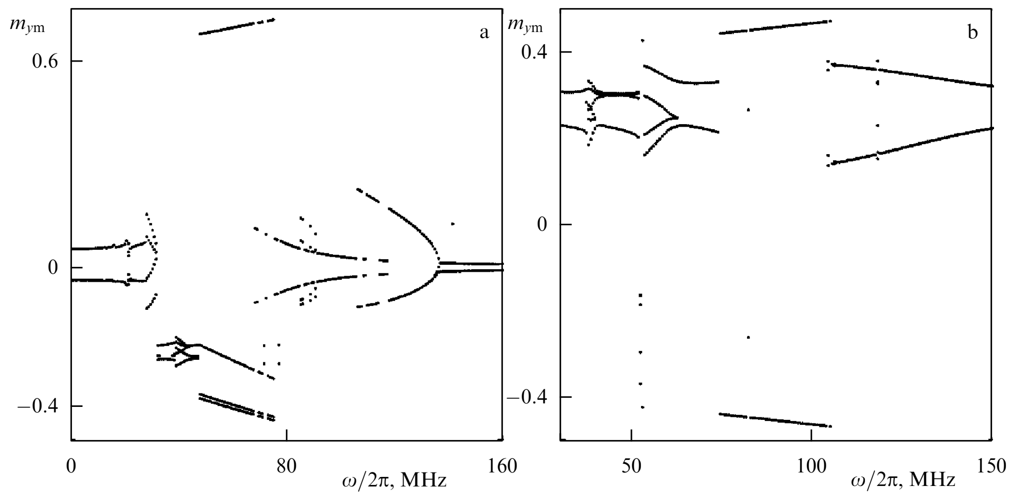

Figure 13. Bifurcation diagrams: frequency dependences of the extrema of the y component of the magnetization precession trajectory for (111) films at $H = 277$ Oe (a) and (100) films at $H = 390$ Oe (b); $h = 1$ Oe, $\varphi_h = 0$, $K_1 = -10^3$ erg cm^{-3}, and $K_u = -10^{-3}$ erg cm^{-3}.

parameters of the ac field (or the magnitude of the dc field), the precession amplitude is only weakly dependent on these parameters. In the zones where the two trajectories alternate (the branches acquire a 'dashed' character), a dynamic bistability is developed, i.e., two stationary precession regimes exist at the same parameters of the system; the development of a particular regime is affected by the initial conditions of the motion. As a rule, the dynamic bistability has hysteretic properties; in the case of a quasi-stationary decrease in the ac field frequency (or the magnetizing field magnitude), one of the precession branches is realized; as the frequency increases, the other branch is realized. Thus, to excite a large-amplitude precession regime, the magnetization vector should be moved from the zone of attraction of the low-amplitude regime, e.g., by its initial shift by using an additional magnetizing field or by the application of an ac field with a somewhat greater amplitude at the first stage of the excitation of the regime. But at the edges of the bistability region, there usually exist narrow zones in which the establishment of a given stationary regime can be affected by fluctuations of the various parameters of the system, in particular, of the initial phase of the ac magnetic field.

Figures 14a and 14b display the yz projections of the trajectories of the magnetization vector in stationary precession regimes that are realized under conditions of dynamic bistability. For (111) films (Fig. 14a), the following parameters were chosen: $h = 1$ Oe, $\omega/2\pi = 7 \times 10^7$ Hz, $H = 277$ Oe, and $K_u = -10^3$ erg cm^{-3} (curves *1*, *2*), and $H = 728$ Oe and $K_u = -5 \times 10^3$ erg cm^{-3} (curves *3*, *4*); and for the (100) films (Fig. 14b): $h = 2$ Oe, $\omega/2\pi = 13 \times 10^7$ Hz, and $H = 1320$ Oe (curves *1*, *2*) and $h = 1$ Oe, $\omega/2\pi = 9.6 \times 10^7$ Hz, and $H = 1420$ Oe (curves *3*, *4*) at $K_u = -10^4$ erg cm^{-3}. The dynamic regimes corresponding to curves *1* and *2* and to curves *3* and *4* are realized at the same parameters of the system, but the establishment of one of the two precession regimes (sometimes strongly differing in amplitude) is strongly affected by the initial phase ζ of the ac magnetic field ($\zeta = 0$ for curves *1* and *3*, and $\zeta = \pi/2$ for curves *2* and *4*). It also follows from the figure that the large-amplitude regimes shown (which are simplest in their trajectories) are characterized by a significant contribution to the dynamics of magnetization from the third harmonic of the precession frequency for the (111) film and from the fourth harmonic for the (100) film; the contributions of these harmonics increase as the amplitude of the ac field increases [32, 59].

Apart from the amplitude bifurcations leading mainly to changes in the magnetization precession amplitude, bifurcations in the sharp changes and a complication of the trajectory of the dynamic regime were revealed. In (111) films, the precession period is often equal to a multiple of the ac field period $T = 2\pi l/\omega$, where l is an integer, whereas in the case of (100) films, the period of the complex trajectory is typically equal to the ac field period: during half the period, the magnetization vector executes several turns about two equilibrium positions, then approaches two other equilibrium positions, and passes around them one or several times during the second half of the period. The curves shown in Fig. 14c correspond to stationary periodic motions of the magnetization with $l = 3$ (solid curve) and $l = 2$ (dashed curves) in the (111) film. In the first case, $h = 2$ Oe, $\omega/2\pi = 4 \times 10^7$ Hz, $H = 502.8$ Oe, and $K_u = -3 \times 10^3$ erg cm^{-3}; in the second case, $h = 1$ Oe, $\omega/2\pi = 3 \times 10^7$ Hz, $H = 728$ Oe, and $K_u = -5 \times 10^3$ erg cm^{-3}. Figure 14d illustrates a relatively rare situation where the period of a complex trajectory in a (100) film is two times that of the ac field ($l = 2$); the parameters of the system were taken as follows: $h = 2$ Oe, $\omega/2\pi = 5 \times 10^6$ Hz, $H = 297$ Oe, and $K_u = 0$. We note that the bifurcations leading to dynamic regimes with a complex trajectory are frequently preceded by stochastic regimes, which are considered in Section 8.

The observed substantial effect of the orientation of crystallographic axes and growth-induced anisotropy on the character of the large-amplitude precession in iron–garnet films allows significantly expanding the variety of dynamic regimes realized in them and the possibilities of their practical application.

8. Stochastic precession in iron–garnet films

In recent years, progressively greater attention is being paid to the investigation of various oscillatory systems characterized by dynamic regimes, along with regular stochastic regimes. This is related not only to the necessity of suppressing chaos and the transfer of initially chaotic systems into a desired regular dynamic regime under the

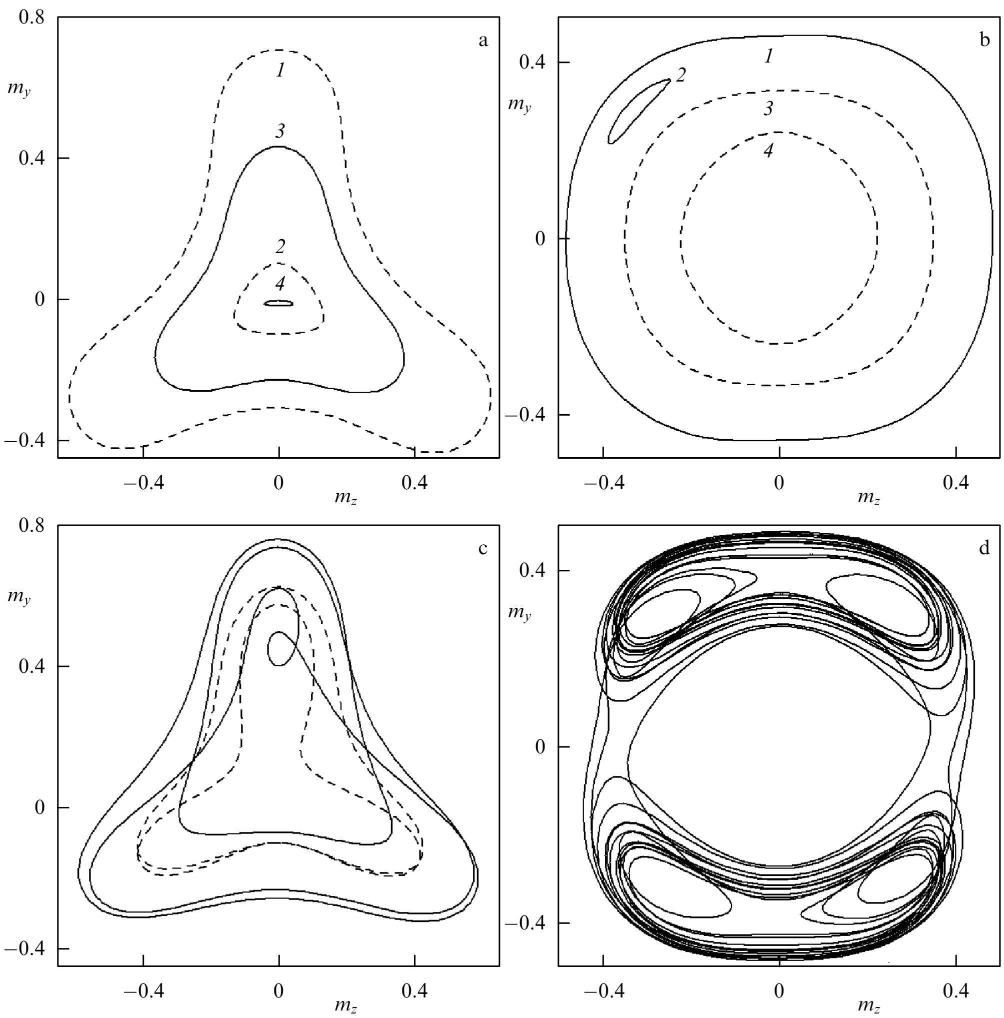

Figure 14. Projections of the trajectories of precessional regimes realized in (111) films (a, c) and (100) films (b, d): (a, b) under conditions of dynamic bistability at the initial phase of the microwave field $\zeta = 0$ (curves *1*, *3*) and $\pi/2$ (curves *2*, *4*); and (c, d) with the the period that is a multiple of the exciting ac field period.

effect of relatively weak actions [90] but also to the possibility of using controlled chaos in advanced technologies. In particular, the results of such investigations have a direct relation to the problems of information processing (recording, coding, and decoding) [91].

An analysis of the dynamics of analogous systems is possible based on considering their phase trajectories, of which the most common are stochastic or quasi-stochastic attractors [92]. Stochastic attractors are a mathematical counterpart of an observed developed chaotic behavior of a physical system with the mixing property [93]. The overwhelming majority of attractors of chaotic dynamic systems belongs to the quasi-stochastic type. Apart from saddle-point limit cycles, such attractors contain stable limit cycles, whose period is sufficiently large and the attraction region is very small. Among the invariants that describe the properties of chaotic systems, there are characteristic Lyapunov exponents and the dimensionality of the strange attractor [94–96].

In the literature, there are reports on the direct observation of bifurcation diagrams and strange attractors during nonlinear oscillations [97] and the results of an experimental study of bifurcation diagrams, including the development of chaos through period doubling in investigations of nonlinear oscillations in semiconductor p–n junctions [98]. The occurrence of regular precession regimes with a doubled, as well as tripled, period with subsequent bifurcations resulting in the period doubling, which are accompanied by a 'quasi-chaotization' (regimes with weakly 'smeared' attractors) and which arise upon an increase in the amplitude of the ac magnetic field, was shown in [25]. For such regimes, $V_{n+1}(V_n)$ diagrams were constructed based on a large amount of experimental data, where V_n is the signal proportional to the rate of change in the transverse magnetization in the sample. The phase portraits and bifurcation diagrams arising in solving the Landau–Lifshitz equations simultaneously with magnetostatic equations for thin films with an insignificant magnetocrystalline anisotropy in an ac field with a circular polarization in the plane perpendicular to the film were analyzed in [99]. The auto-oscillation and stochastic regimes of the magnetization precession in iron–garnet films were typically investigated in the case of the development of spin-wave instabilities [7, 25, 100, 101].

The stochastic and quasi-periodic dynamics of the uniformly precessing magnetization, which is established in crystals with a uniaxial anisotropy in weak magnetizing fields at frequencies that are less than the linear resonance frequency, have been considered in [31]

To study the stochastic dynamic regimes and the transitions between them in more detail and to analyze the regular regimes in uniformly magnetized structures under the above-mentioned conditions, we consider (111) and (100) films [102]. The simultaneous consideration of films of two types allows revealing the effect of the magnetocrystalline anisotropy of the material on the establishment of these regimes and analyzing their common features.

The most complete information on the character of dynamic regimes in the structure under consideration can be obtained in a wide range of values of a given parameter from a bifurcation diagram [103, 104]. Figure 15 shows the bifurcation diagrams on the (m_{ym}, H) plane for (111) films (Figs 15a, b) and (100) films (Figs 15c, d). It follows from these diagrams that at a fixed value of H, there are two points corresponding to a regular oscillatory regime with one maximum $(m_{y\,\max})$ and one minimum $(m_{y\,\min})$, whose nonlinear character manifests itself only in a nutational motion; the greater but finite number of points corresponds to a more complex oscillation, and the set of closely located points corresponds to the stochastic dynamics of the magnetization. For a numerical analysis, we took the range of the magnetizing field near the value corresponding to linear resonance at relatively small frequencies of the ac field. The following parameters of the system were used in the calculations: the transverse ac field amplitude $h = 1$ Oe (Figs 15a, b) and $h = 2$ Oe (Figs 15c, d); the ac field frequency $\omega/2\pi = 4 \times 10^7$ Hz; and the magnetocrystalline and growth-induced anisotropy constants $K_1 = -10^3$ erg cm^{-3} and $K_u = -3 \times 10^3$ erg cm^{-3}. The investigations showed that for the (111) films, the stochastic dynamics occurs at frequencies $\omega/2\pi \approx (2-50) \times 10^6$ Hz. At frequencies above this range, only regular precession of magnetization is established; at frequencies below this range, regimes of switching between equilibrium orientations arise. The stochastic precession in (100) films is also realized at significantly lower frequencies.

We see from Fig. 15 that in approaching the zone of stochastic dynamics from the side of larger values of the magnetizing field, an increase in the amplitude of regular precession (in some cases accompanied by a complication of the precession trajectory) is first observed. After the development of stochasticity (with a further decrease in H), the precession amplitude continues increasing and the corresponding attractors are gradually modified. From the side of the smaller values of the magnetizing field, the zone of stochastic regimes is bounded by low-amplitude regular oscillations. In this case, a sharp decrease in the precession amplitude occurs. In the stochasticity zone, the regions of stochastic regime typically alternate with much narrower regions corresponding to regular regimes. However, no qualitative changes were found in the attractor of stochastic oscillations after passing through the region of regular precession in these structures. The greatest precession amplitude, i.e., the lower boundary of the zone under consideration, may correspond to both stochastic and

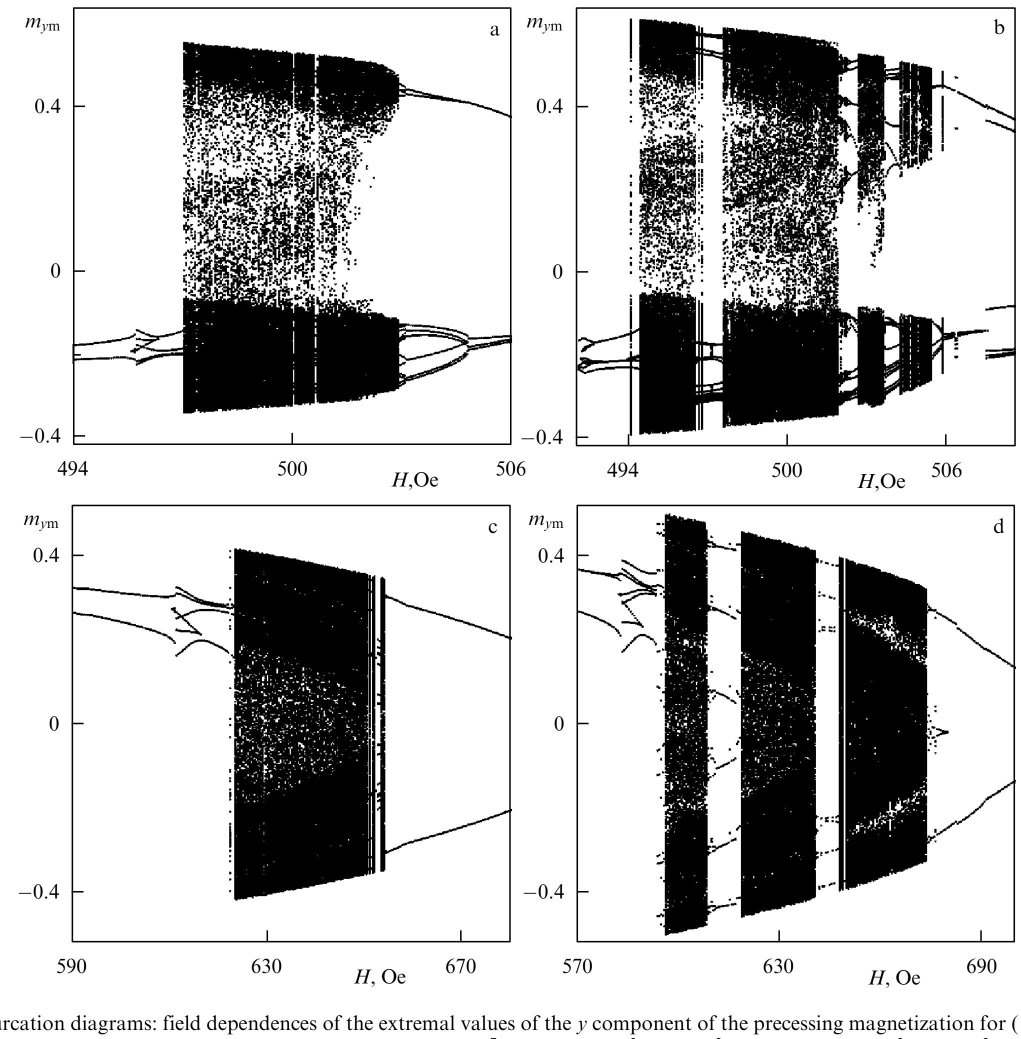

Figure 15. Bifurcation diagrams: field dependences of the extremal values of the y component of the precessing magnetization for (111) films (a, b) and (100) films (c, d) at $h = 1$ Oe (a, c) and $h = 2$ Oe (b, d); $\omega/2\pi = 4 \times 10^7$ Hz, $K_1 = -10^3$ erg cm^{-3}, and $K_u = -3 \times 10^3$ erg cm^{-3}.

regular regimes. An increase in the ac field amplitude leads to an expansion of the stochasticity zone and its complication; an increase in both the number and width of regions corresponding to complex precession regimes is observed. Analysis also shows that in contrast to (100) films, the stochastic regimes in (111) films are established at smaller values of the magnetizing field, and the stochasticity zone is smaller by almost an order of magnitude; in (111) films, this zone lies in an interval about $\Delta H \sim 1$ Oe wide, whereas for (100) films, this interval is $\Delta H \sim 10$ Oe. With increasing the growth-induced anisotropy field, the realization of stochastic regimes in (111) films stops much earlier than in (100) films. Thus, at $K_u = -10^3$ erg cm^{-3}, the ac field with the amplitude $h = 1$ Oe excites the stochastic dynamics of magnetization only in the second case.

For clarity, it is convenient to represent the phase trajectories corresponding to stochastic dynamics in the form of a set of points obtained in time intervals equal to the period or half-period of the ac field (an analog of Poincaré diagrams [95, 103]). Figure 16 shows discrete representations (with the time step $\Delta t = \pi/\omega$) of yz projections of the magnetization trajectories for (111) films (Figs 16a, b) and (100) films (Figs 16c, d) at different values of the magnetizing field H (indicated in the figure caption), the ac field amplitude $h = 2$ Oe, and the other parameters corresponding to Fig. 15. The attractors shown are fractals with different fractal dimensions. The stochasticity in this case can involve various angular intervals of precession. As a result, the degree of chaos in the corresponding dynamic regimes is also different; it is determined by the largest Lyapunov exponent and is controlled by changing the magnetizing field magnitude (or parameters of the ac magnetic field).

In the above cases, the stochastic regimes are developed from a regular precessional dynamics with a large contribution from the nutation motion in the third and fourth harmonics of the precession frequency, because we are considering single-crystal films with a cubic magnetocrystalline anisotropy. The stochastic dynamics in structures with a uniaxial anisotropy were investigated in [31, 55]. In particular, the authors of [55] considered the development of stochasticity in a thin polycrystalline nanoelement under the effect of a spin-polarized current. In this case, the stochastic attractor was developed from the magnetization trajectory with a large contribution of nutation motion at the doubled precession frequency.

9. Stochastic oscillations of magnetization in metallic sublattices

Investigations of nonlinear regular and stochastic dynamic magnetization regimes (and transitions between them) in magnetically coupled systems, such as multilayer or multi-

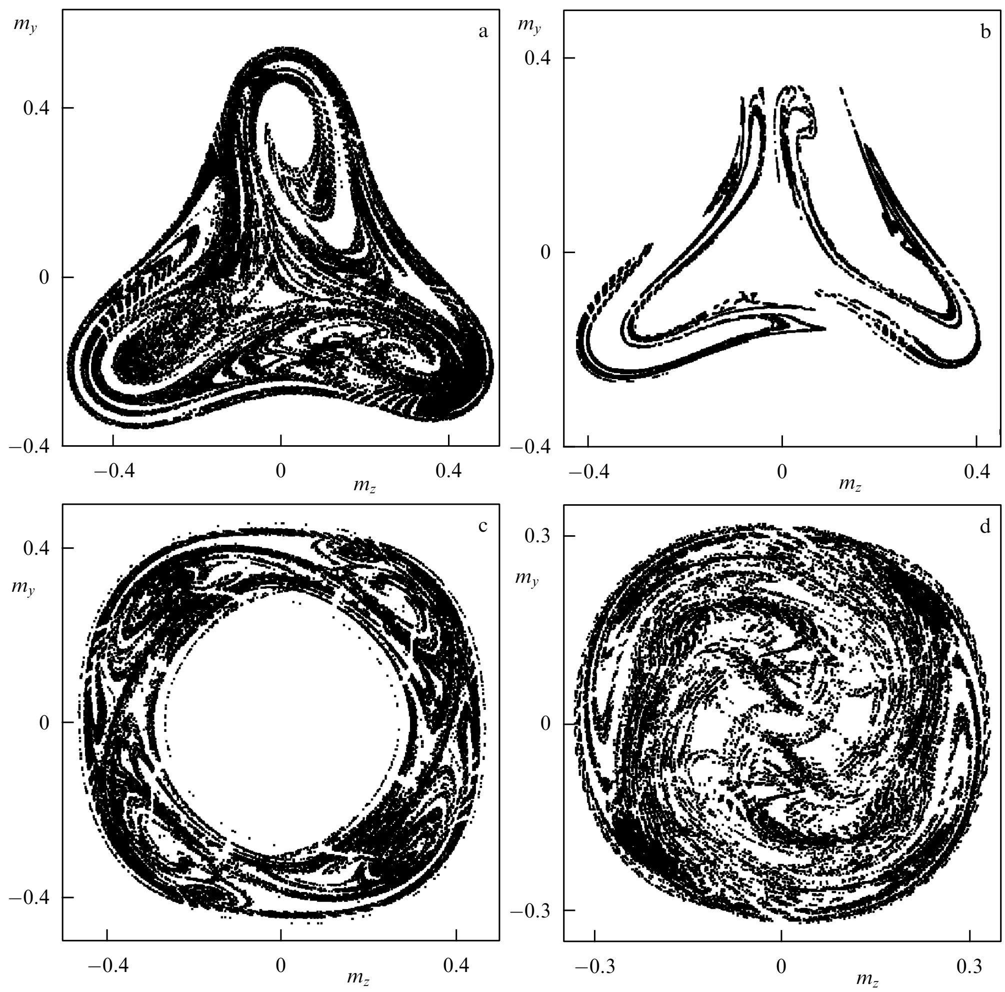

Figure 16. Discrete representation (with the time step $\Delta t = \pi/\omega$) of the yz projections of the magnetization trajectories for (111) films (a, b) and (100) films (c, d) at $H = 496$, 503, 600, and 660 Oe (Figs 16a – d, respectively); $h = 2$ Oe.

domain structures or systems with coupled modes of spin and magnetostatic waves, are presently important from both theoretical and practical standpoints. In [105], a numerical analysis was used to study transitions between stochastic and regular oscillations in an open nonconservative system of two plane coplanar magnetized bodies possessing moments of inertia; however, the authors used essential simplifications (such as the approximation of the in-plane motion of magnetic moments and dipole–dipole interaction of two magnetized layers), which do not necessarily adequately reflect the nonlinear dynamics of real structures. The development of chaotic motion in a system of two interacting magnetic moments in an external magnetic field was analyzed within classical and quantum approaches in [106], where strange attractors were constructed for various applied fields and a suggestion was made regarding the development of more pronounced chaos in coupled ferromagnetic lattices. The nonlinear (in particular, stochastic) dynamics of a periodic system of interacting domain walls in magnetic films described in terms of the Poincaré plane were analyzed in [107]. The authors noted that the results of calculations have a universal character for uniaxial highly anisotropic ferromagnetic films with a stripe-domain structure, because the results obtained can simply be recalculated for materials with different magnetic characteristics. Universal chaotic phenomena, in particular, the development of chaos through a cascade of period doublings, were revealed in the case of interaction of two spin-wave modes in a thin metallic film [108]. In [109], the chaotization of spin waves in a two-layer magnetically coupled structure at a high level of excitation by a spin-polarized current was investigated.

We now consider transitions between nonlinear regular and stochastic precessional regimes that are realized under the effect of a longitudinal ac magnetic field in a multilayer metallic nanostructure $(\mathrm{Fe/Cr})_n$ with an antiferromagnetic interlayer exchange coupling [110, 111].

As shown in Section 5, at small values of the coupling constant J in sublattices with an antiferromagnetic interaction, a change in the magnitude of the magnetizing field is accompanied by the development of loops of orientational hysteresis and related bistability states. With increasing coupling constants, the hysteresis loop becomes narrower and collapses at $J = J_{\mathrm{ab}}$, where J_{ab} is found from the equality $H_{\mathrm{b}} = H_{\mathrm{a}}$ [see Eqns (17)]. At the values of H corresponding to the middle of the hysteresis loop, the application of a longitudinal high-frequency field ($\mathbf{h} \parallel \mathbf{H}$) with the amplitude close to the hysteresis width ($h \geqslant H_{\mathrm{a}} - H_{\mathrm{b}}$) leads to the development of various high-amplitude auto-oscillating and stochastic regimes in the system of magnetic moments of the layers. Thus, as regards the possibility of the realization of various dynamic regimes, systems with narrow hysteresis loops are of special interest.

Figure 17 displays a bifurcation diagram (with the ac field frequency plotted along the abscissa axis and the corresponding extremal values of the angles of the magnetic moments of the first subsystem along the ordinate axis) for the exchange coupling constant $\bar{J} = 0.24$ erg cm^{-2} (close to the value $\bar{J}_{\mathrm{ab}} \approx 0.244$ erg cm^{-2}), the magnetizing field $H = 2227.4$ Oe (at which a collinear equilibrium state with angles $\varphi_{0j} = 0$ is realized), and the ac field amplitude $h = 0.2$ Oe, which exceeds the value $H_{\mathrm{a}} - H_{\mathrm{b}} \approx 0.144$ Oe. The oscillations of the magnetic moments of the two subsystems are always in antiphase and the equality $\varphi_2(t) = -\varphi_1(t)$ is satisfied with a great accuracy in both regular and stochastic regimes. As the

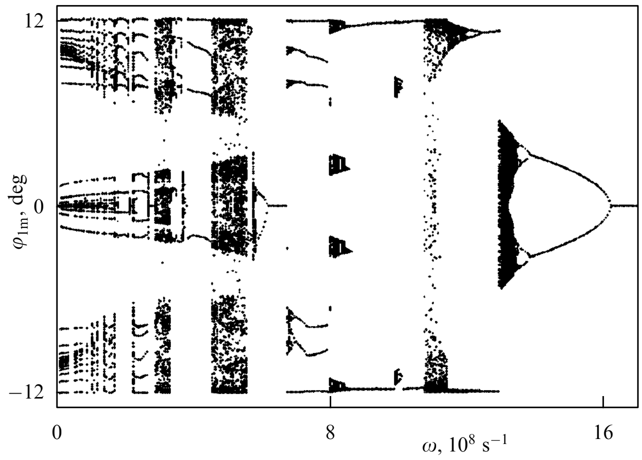

Figure 17. Frequency dependence of the maximum and minimum values of the angle φ_1 (bifurcation diagram) at $h = 0.2$ Oe, $\bar{J} = 0.24$ erg cm^{-2}, and $H = 2227.4$ Oe.

frequency changes, the transformation of one set of regular oscillation regimes into others is seen to be realized, as a rule, through the passage of frequency intervals corresponding to the stochastic dynamics of magnetic moments. Among regular regimes, both symmetric and asymmetric (with respect to the axis with a zero value of the azimuthal angle) regimes exist.

If we investigate the diagram from the side of greater frequencies, we see that the system is initially unsusceptible to the effect of an ac field. Then, after a Hopf bifurcation [103], a limit cycle arises with an amplitude that increases with decreasing the frequency. Further, after a period-doubling cascade, a stochastic oscillatory regime is developed in the system. When the amplitude of stochastic oscillations becomes sufficiently large, the magnetic moments enter the zone of attraction of an attractor, which represents a high-amplitude limit cycle; this leads to a new bifurcation and the establishment of an auto-oscillating regime. Large-amplitude oscillations can also arise at higher frequencies, but in the case of a different initial orientation of magnetic moments, i.e., dynamic bistability arises in a certain frequency range. At large ac field amplitudes (e.g., $h = 1$ Oe), the stochastic dynamics have no time to develop, because the value of the deviation angle φ_j in the case of a low-amplitude limit cycle arising after the Hopf bifurcation is sufficiently large for the magnetic moments to be attracted by the attractor of the auto-oscillating regime [110].

The amplitude of the auto-oscillating regime only weakly depends on the ac field frequency and in all cases significantly exceeds the difference between the angles of the magnetic moments in the hysteresis loop ($\varphi_{\mathrm{a}} \approx 6°$). Although the oscillation amplitude depends on h, this dependence is sufficiently weak; a fivefold increase in h leads to an increase in the amplitude of the angle φ_1 by only one-third. However, the frequency region corresponding to a given regular regime significantly expands with an increase in the ac field and is shifted toward higher frequencies.

As the frequency decreases, the regular oscillations again change into stochastic ones. At a sufficiently small deviation from the frequencies corresponding to the regular dynamics, the amplitude of oscillations is bounded in a certain range of angles, which leads to a smearing of the limit cycle phase

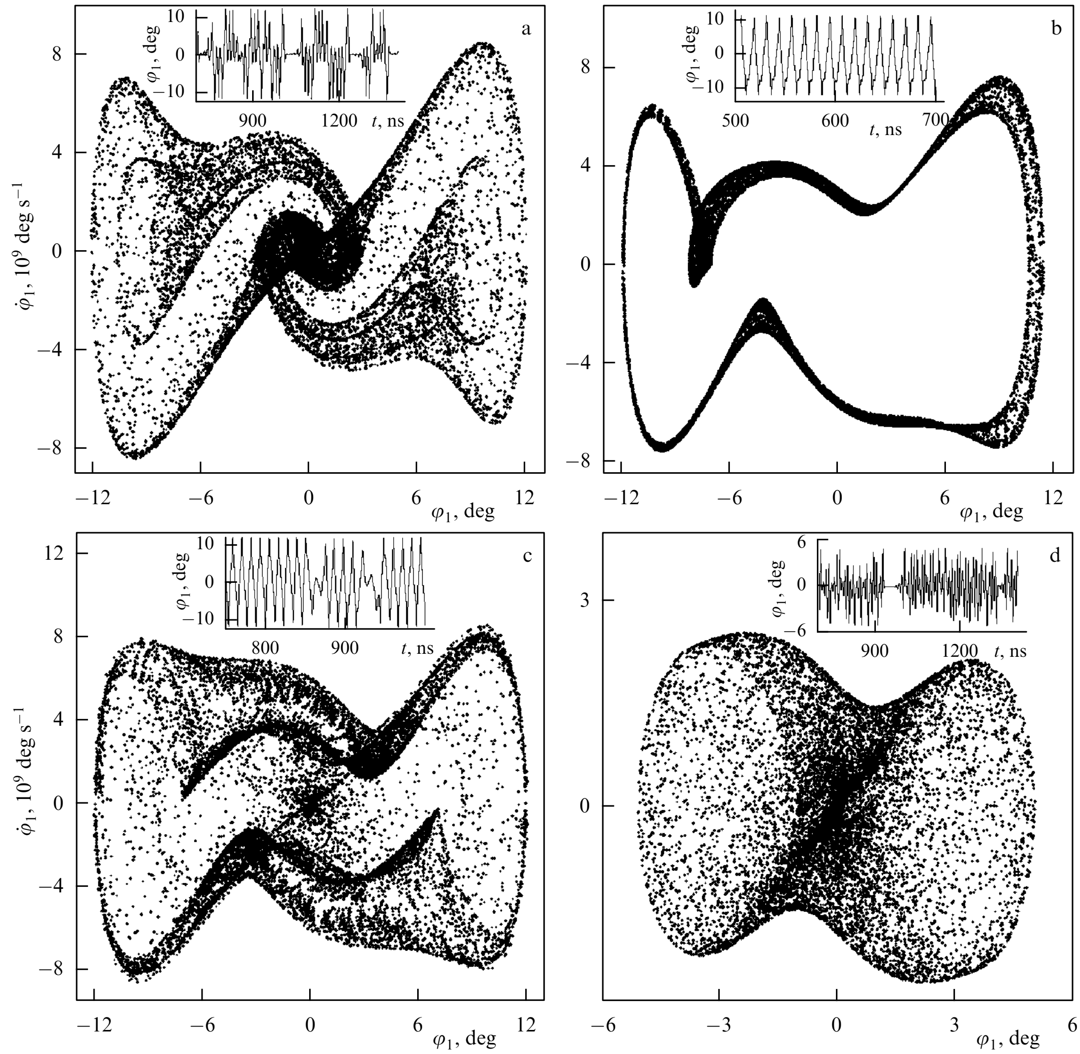

Figure 18. Discrete representation (with the time step $\Delta t = \pi/\omega$) of the phase trajectories of the magnetic moment at $h = 0.2$ Oe: $\omega = 5.0 \times 10^8$ c^{-1} (a), $\omega = 9.95 \times 10^8$ c^{-1} (b), $\omega = 11.0 \times 10^8$ c^{-1} (c), and $\omega = 13.1 \times 10^8$ c^{-1} (d); the insets show the $\varphi_1(t)$ dependences.

trajectory. With a further decrease in frequency, the stochasticity becomes more pronounced and the attractor of oscillations becomes thicker, involving the entire range of oscillations of the magnetic moment angle at the frequency $\omega = 11 \times 10^8$ s^{-1}; the stochastic regime in this case exhibits 'laminar' regions, which alternate with bursts of 'turbulence' [95].

Along with wide frequency regions corresponding to stochastic oscillations, the diagram contains narrow frequency intervals ($\Delta\omega \sim 10^7$ s^{-1}) in which stochastic regimes are realized, with regular large-amplitude regimes observed outside these intervals. As the frequency decreases, stochastic regimes are established after a cascade of period-doubling bifurcations; the passage of the system into an auto-oscillating regime with the period equal to that of the ac field occurs after a single bifurcation. The regular regimes at frequencies below and above the frequency interval corresponding to the stochastic dynamics can be both very close and significantly different in their phase trajectories.

Apart from frequency intervals corresponding to stochastic and regular oscillations, there also exist frequency intervals of dynamic insusceptibility (e.g., at $h = 0.2$ Oe near the frequency $\omega = 6.5 \times 10^8$ s^{-1}), which narrow and finally vanish with increasing h. At small frequencies ($\omega \sim 10^7$ s^{-1}), regular dynamic regimes exist that are characterized by the presence of time intervals with a zero angle and fast oscillations related to the magnetization reversal.

Figure 18 shows discrete images (constructed using time steps equal to half the ac field period) of phase portraits of stochastic dynamics of the magnetic moment at $h = 0.2$ Oe and various values of ω; the insets show corresponding $\varphi_1(t)$ dependences. The dynamic regime near the frequency $\omega = 5.0 \times 10^8$ s^{-1} (Fig. 18a) arises as a result of a passage through the [100] intermittence, but the 'laminar' phases (large-amplitude oscillations of the angle in either the positive or negative half-plane) include only a few periods. The phase portrait of this regime is given by a combination of two funnel-type attractors between which the transition occurs in the central region of the phase plane.

The regime corresponding to the frequency $\omega = 1.1 \times 10^9$ s^{-1} (Fig. 1c) also has 'laminar' phases, which alternate with bursts of 'turbulence' and are characterized by a certain angular interval of the spread in the oscillation amplitude. With increasing the frequency, the turbulence bursts disappear and a stochastic regime with an attractor that does not touch the central region of the phase plane is established. In Fig. 18b, the stochasticity manifests itself only in the smallness of the interval of the magnetic moment azimuthal angle and its first derivative, i.e., in a small smearing of the limit cycle trajectory. This regime has an asymmetric attractor and is realized in a narrow frequency interval (see Fig. 17). In Fig. 18d, the stochastic dynamics were developed as a result of a period-doubling cascade and after the reverse cascade [95] corresponding to the merging of 'noise' intervals of the angle φ_1; therefore, the stochasticity involves the entire angular range of oscillations of the magnetic moment.

The attractors corresponding to the stochastic dynamics of magnetization have regions of a strong contraction or folds and regions of expansion. This makes the phase trajectories sensitive to the initial conditions. Figure 19 presents, for the cases shown in Fig. 18, the time dependences of the logarithm of the relative spacing $\ln(\delta/\delta_0)$ between two points of phase trajectories of the magnetic moment $\mathbf{M}_1$ chosen in the plane $(\varphi_1, \dot{\varphi}_1)$ located closely to one another at the initial instant ($\delta = \delta_0$ at $t = 0$). The curves given are shifted along the time axis, because for each of them its own initial time was chosen for convenience. It can be seen from the dependences shown that the distance between the points first increases on average in accordance with the exponential law $\delta = \delta_0 \exp(\xi t)$, where ξ is the largest Lyapunov exponent equal to the slope of the straight line approximating the divergence of the phase trajectories (dashed line intersecting curve *1*). After reaching the scales of the attractor, δ begins oscillating about the value determined by the size of the attractor. An analysis of the phase portraits of the corresponding regimes shows that with an expansion of the attractor, i.e., with increasing 'noise' intervals, the Lyapunov exponent increases. When the attractor includes the central region of the phase plane (curves *a*, *b*, *c*), the divergence rate of the closely located trajectories becomes significantly greater than the stochasticity and manifests itself only in a smearing of the limit cycle trajectory (curve *b*). At $\omega = 11 \times 10^8$ s^{-1} (curve *c*), the divergence rate of the trajectories is determined by two rates: the small rate in the laminar phase and the high rate during the bursts of 'turbulence.' As the frequency increases, the duration of the laminar phases increases, and therefore the rate decreases and the $\delta(t)$ dependence becomes smoother. In the cases considered, $\zeta \approx 12.7 \times 10^7$ s^{-1} (curve *a*), 3.8×10^7 s^{-1} (curve *b*), 9.8×10^7 s^{-1} (curve *c*), and 15.2×10^7 s^{-1} (curve *d*).

The period-doubling cascade for structures with two interacting subsystems has some specific features. The bifurcation diagram of this subharmonic cascade shown in Fig. 20 (with parameters corresponding to Fig. 17) is divided into three frequency regions; in regions I and III, the magnetic moments of both subsystems oscillate symmetrically with respect to the zero value of the azimuthal angle and, consequently, the angular ranges in which the $\varphi_j(t)$ dependence is realized are equal for $\mathbf{M}_1$ and $\mathbf{M}_2$; in region II, the oscillations of the magnetic moments are asymmetric and the above ranges are different [the branches corresponding to the first ($j = 1$) and second ($j = 2$) subsystems are marked by *1* and *2*]. We see from the diagram that a Hopf bifurcation (the generation of a limit cycle from fixed point in the phase plane) is the first to appear; however, the next bifurcation, arising at $\omega \approx 13.83 \times 10^8$ s^{-1}, does not lead to a period doubling (as in the case of a subharmonic cascade in many other systems) but causes a shift of the angular intervals of the magnetic moment oscillations, i.e., to the appearance of an asymmetry in their dynamics. For the vector of the total magnetization of the structure $\mathbf{M} = \mathbf{M}_1 + \mathbf{M}_2$, this bifurcation is a Hopf bifurcation, because in the region preceding it, the variable components of the magnetization of the two subsystems of layers compensate each other.

A further decrease in the frequency leads to a cascade of bifurcations corresponding to period doubling in the dynamics of each of the magnetic moments and to the appearance of stochastic oscillations. At the beginning of the reverse cascade, the asymmetry of the dynamics of magnetic moments is retained: for different magnetic subsystems, the extrema of the $\varphi_j(t)$ dependence are located in different angular ranges. At the frequency $\omega \approx 13.42 \times 10^8$ s^{-1}, a bifurcation occurs due to which the stochastic oscillations of the magnetization of both subsystems begin to include equal angular ranges located symmetrically with respect to the zero value. Thus, in the structure under consideration, the application of a longitudinal ac magnetic field in a subharmonic cascade prior to the appearance of period doubling bifurcations leads to the generation of an additional bifurcation related to a symmetric shift of the

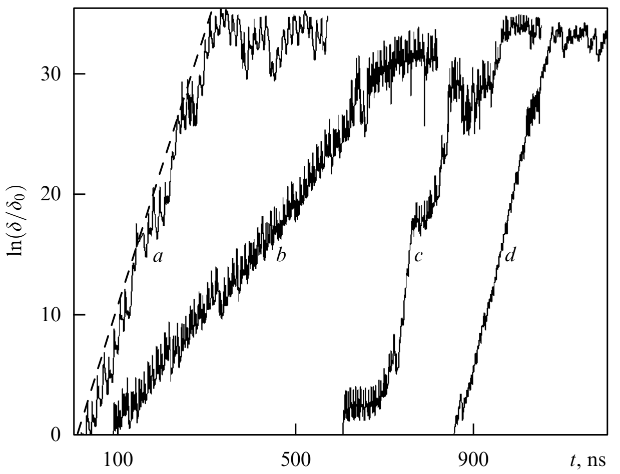

Figure 19. Time dependences of the spacing between two phase points closely located at the initial instant.

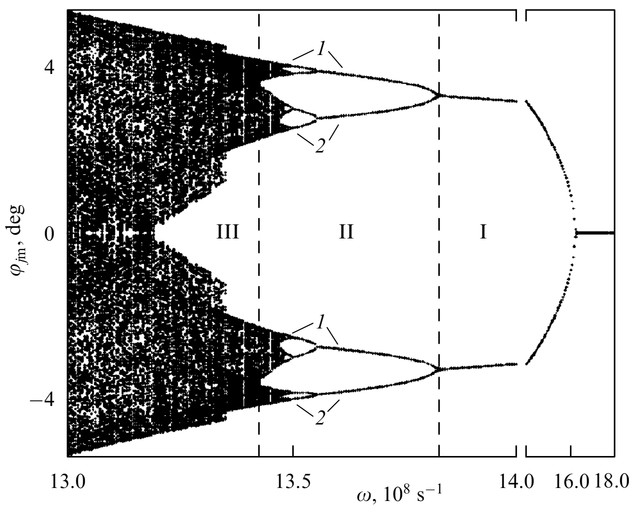

Figure 20. Bifurcation diagram of the frequency dependence of the extremal values of the angles φ_j for a period-doubling cascade.

angular range of magnetic moment oscillations. During the reverse cascade, bifurcations that induce a jumplike increase in the stochasticity of the dynamics are realized.

As regards various features of the formation of chaos after a period doubling cascade, we note paper [108], whose authors studied spin-wave dynamics and obtained chaotic regimes lying in the bifurcation diagram in the region between two subharmonic cascades directed to the opposite sides with respect to the magnitude of the control parameter.

For practical applications, the problem of transition between regular and stochastic dynamic regimes caused by various external effects on the system is greatly important. The analysis performed shows that as the ac field amplitude changes, the transformation of the regular oscillating regime from one type to another is typically realized via the field h passage through the regions corresponding to the stochastic dynamics of magnetic moments. Among regular regimes, there exist regimes that are either symmetric or asymmetric with respect to the axis with a zero value of the azimuthal angle. Thus, when the stochastic oscillating regime in the system is realized via a sufficiently small change in the amplitude of h ($\Delta h < 0.1$ Oe), as well as in the case of a small change in the ac field frequency, the system can be brought into one of the regular dynamic regimes. The various transitions between regular and stochastic regimes also occur upon changes in the magnitude of the magnetizing field.

With the relations $4\pi M^2 \gg 2K_1$ and $\lambda \ll \gamma M$, which are satisfactorily fulfilled for metallic magnetic films, the set of equations of motion for magnetic moments (1) can be reduced to [24]

$$\ddot{\varphi}_j + 4\pi\lambda\dot{\varphi}_j + 4\pi\gamma^2 \frac{\partial F}{\partial \varphi_j} = 0\,, \quad \dot{\psi}_j = -\frac{\ddot{\varphi}_j}{4\pi M_j}\,. \tag{26}$$

In the case of a symmetric orientation of the magnetizing and high-frequency fields with respect to the axes of the magnetocrystalline and growth-induced anisotropy and with the antiferromagnetic character of the coupling between magnetic moments of neighboring layers, their precession angles are antisymmetric ($\psi_1 = -\psi_2 = \psi, \varphi_1 = -\varphi_2 = \varphi$). As a result, the set of four equations (26) reduces to two equations for φ and ψ. A further simplification is related to the smallness of the angles of the deviation of the magnetic moments from the in-plane position (for the system parameters used, this angle is $\psi(t)_{\max} \sim 0.01^\circ$). Because $\psi \approx 0$, the derivative $\partial F/\partial\varphi$ loses its dependence on ψ; in analyzing the azimuthal motion, this allows replacing the spatial precession of magnetic moments by their in-plane oscillation. As a result, we obtain the following equation for the azimuthal angle:

$$\ddot{\varphi} + 4\pi\lambda\dot{\varphi} + 4\pi\gamma^2\big[(H + h\sin\omega t)\,M\cos\varphi + (K_1\cos 2\varphi - \bar{J}\,)\sin 2\varphi\big] = 0\,. \tag{27}$$

A comparative analysis shows that the use of approximate equation (27) for describing the precession dynamics of magnetic moments of magnetically coupled multilayer systems leads to solutions that differ substantially from those above in some frequency ranges. Nevertheless, many auto-oscillating and stochastic regimes were obtained by solving a single equation for the angle φ.

The above-considered model of a multilayer structure is simplified. Apart from the roughness of the interlayer interfaces, real structures also involve deviations of the coupling coefficients and magnetizations from their mean values, which occur, in particular, due to the existence of structure defects and the finite number of layers in the system. In addition, the character of the interlayer coupling can differ from the bilinear exchange interaction [72]. Taking all these factors into account can substantially complicate the analysis of the nonlinear regular and stochastic dynamics of magnetic moments and lead to a significant increase in the variety of the arising dynamic regimes. Nevertheless, the results presented above correctly reflect the main features of the dynamic behavior of real multilayer systems under conditions where narrow hysteresis loops are realized; these results are also valid for bilayer systems of the 'sandwich' type with the antiferromagnetic coupling.

10. Conclusions

The results of investigations of the nonlinear precession dynamics of magnetization in thin-film magnetic structures given in this review can be summarized as follows. The nonlinear character of the precessional motion causes the appearance of regions of the system parameters in which various types of bifurcations are realized, leading to a changeover of a dynamic regime and to the occurrence of a dynamic bistability. The most common of these are large-amplitude auto-oscillating and stochastic regimes related to the existence of bistability states and orientational jumps or more complex precessional motions of the magnetization vector between several equilibrium positions, which are realized under the effect of an ac magnetic field. The amplitude of these precession regimes in a sufficiently wide range of parameters of the ac field only weakly depends on these parameters. The arising stochastic regimes differ strongly in both the degree of stochasticity and the fractal dimensionality of the attractor, which can easily be controlled; in addition, transitions between regular and stochastic dynamic regimes can be effected by changing the parameters of external magnetic fields.

In normally magnetized ferrite films with a cubic magnetocrystalline anisotropy, the auto-oscillating and stochastic regimes of the magnetization precession are established under conditions corresponding to the development of orientational bistability at frequencies that are much lower than that of the linear resonance. The amplitude of these regimes is mainly determined by the orientations of the magnetization in equilibrium. A change in the orientation of the magnetocrystalline anisotropy axes qualitatively changes the arising dynamic regimes (the shape of the attractors and related frequency ranges) and also affects the possibility of controlling the nonlinear (including stochastic) regimes with the help of external fields.

In metallic multilayer structures with the antiferromagnetic coupling at the parameters corresponding to the edge of the orientational hysteresis loop in a transverse microwave field, a dynamic magnetization reversal of the system is realized; in this case, frequency intervals depending on the magnetic field appear, which correspond to a precession bistability, i.e., to a state with two possible strongly differing precession regimes. In systems with a narrow hysteresis loop, various types of large-amplitude auto-oscillating and stochastic regimes are established under the effect of a longitudinal ac magnetic field. At magnetizing fields and microwave field frequencies close to values corresponding to the intersection of the 'acoustic' and 'optical' resonance branches, an asymmetric oscillating regime is realized that is characterized by a strong difference in the magnetic moment amplitudes of oscillation of neighboring layers and can easily be controlled by changing the in-plane angle of the ac field.

To conclude, we note that this review is one of the first attempts at generalizing the various nonlinear precession regimes that are realized in thin-film magnetic structures and are characterized by dynamics that are homogeneous over the sample. But presenting the available results was by no means the only purpose of the review. It is known that the absence of a generalizing analysis always hinders an efficient scientific search and the available generalizations are always insufficient. Therefore, one of the aims of this review was also to stimulate further investigations in this field.

Acknowledgments. This work was supported in part by the Grant of the President of the Russian Federation No. MD-3169.2007.2.

References

1. Monosov Ya A *Nelineinyi Ferromagnitnyi Rezonans* (Nonlinear Ferromagnetic Resonance) (Moscow: Nauka, 1971)
2. L'vov V S *Nelineinye Spinovye Volny* (Nonlinear Spin Waves) (Moscow: Nauka, 1987)
3. Bryant P H, Jeffries C D, Nakamura K *Phys. Rev. A* **38** 4223 (1988)
4. Kandaurova G S, Sviderskiĭ A É *Pis'ma Zh. Eksp. Teor. Fiz.* **47** 410 (1988) [*JETP Lett.* **47** 490 (1988)]
5. Kaganov M I, Pustyl'nik N B, Shalaeva T I *Usp. Fiz. Nauk* **167** 191 (1997) [*Phys. Usp.* **40** 181 (1997)]
6. Neite B, Dötsch H *J. Appl. Phys.* **62** 648 (1987)
7. Rezende S M, de Aguiar F M *Proc. IEEE* **78** 893 (1990) [*TIIER* **78** (6) 5 (1990)]
8. Lisovskii F V et al. *Zh. Eksp. Teor. Fiz.* **103** 213 (1993) [*JETP* **76** 116 (1993)]
9. Chaplygin Yu A (Ed.) *Nanotekhnologii v Elektronike* (Nanotechnologies in Electronics) (Moscow: Tekhnosfera, 2005)
10. Chui S T *Phys. Rev. B* **55** 3688 (1997)
11. Filippov B N *Fiz. Nizk. Temp.* **28** 991 (2002) [*Low Temp. Phys.* **28** 707 (2002)]
12. Waintal X, Parcollet O *Phys. Rev. Lett.* **94** 247206 (2005)
13. Xiao D, Tsoi M, Niu Q *J. Appl. Phys.* **99** 013903 (2006)
14. van Saarloos W *Phys. Rep.* **386** 29 (2003)
15. Weinan E, Weiqing R, Vanden-Eijnden E, cond-mat /0205168
16. Liu W-M et al. *Phys. Rev. E* **54** 4612 (1996)
17. Bertotti G et al. *J. Appl. Phys.* **91** 7559 (2002)
18. Logunov M V, Gerasimov M V *Fiz. Tverd. Tela* **44** 1627 (2002) [*Phys. Solid State* **44** 1703 (2002)]
19. Mal'tsev V N, Kandaurova G S, Kartagulov L N *Fiz. Tverd. Tela* **45** 658 (2003) [*Phys. Solid State* **45** 691 (2003)]
20. Prokhorov A M, Smolenskiĭ G A, Ageev A N *Usp. Fiz. Nauk* **143** 33 (1984) [*Sov. Phys. Usp.* **27** 339 (1984)]
21. Zvezdin A K, Kotov V A *Magnitooptika Tonkikh Plenok* (Magnetooptics of Thin Films) (Moscow: Nauka, 1988)
22. Stashkevich A A *Izv. Vyssh. Uchebn. Zaved., Fiz.* **32** (4) 5 (1989)
23. Sementsov D I, Shutyi A M *Opt. Spektrosk.* **84** 280 (1998) [*Opt. Spectrosc.* **84** 238 (1998)]
24. Gurevich A G, Melkov G A *Magnitnye Kolebaniya i Volny* (Magnetic Oscillations and Waves) (Moscow: Fizmatlit, 1994); *Magnetization Oscillations and Waves* (Boca Raton: CRC Press, 1996)
25. Gibson G, Jeffries C *Phys. Rev. A* **29** 811 (1984)
26. Wigen P E et al. *J. Appl. Phys.* **63** 4157 (1988)
27. de Aguiar F M, Azevedo A, Rezende S M *Phys. Rev. B* **39** 9448 (1989)
28. Rezende S M, Azevedo A *Phys. Rev. B* **45** 10387 (1992)
29. Tikhonov V V, Tolkachev A V *Fiz. Tverd. Tela* **36** 185 (1994) [*Phys. Solid State* **36** 101 (1994)]
30. Zil'berman P E, Temiryazev A G, Tikhomirova M P *Zh. Eksp. Teor. Fiz.* **108** 281 (1995) [*JETP* **81** 151 (1995)]
31. Álvarez L F, Pla O, Chubykalo O *Phys. Rev. B* **61** 11613 (2000)
32. Shutyĭ A M, Sementsov D I *Zh. Eksp. Teor. Fiz.* **118** 610 (2000) [*JETP* **91** 531 (2000)]
33. Shutyi A M, Sementsov D I *Fiz. Tverd. Tela* **42** 1268 (2000) [*Phys. Solid State* **42** 1306 (2000)]
34. Gulyaev Yu V *Fiz. Tverd. Tela* **42** 1962 (2000) [*Phys. Solid State* **42** 1094 (2000)]
35. Krupicka S *Physik der Ferrite und der verwandten magnetischen Oxide* (Prag: Academia, 1973) [Translated into Russian, Vol. 2 (Moscow: Mir, 1976)]
36. Kazansky A K, Uzdin V M *Phys. Rev. B* **52** 9477 (1995)
37. Gnatzig K et al. *J. Appl. Phys.* **62** 4839 (1987)
38. Prabhakar A, Stancil D D *J. Appl. Phys.* **85** 4859 (1999)
39. Fetisov Yu K, Patton C E *Radiotekh. Elektron.* **45** 735 (2000) [*J. Commun. Technol. Electron* **45** 664 (2000)]
40. Sementsov D I, Shutyi A M *Pis'ma Zh. Eksp. Teor. Fiz.* **75** 287 (2002) [*JETP Lett.* **75** 242 (2002)]
41. Randoshkin V V, Chervonenkis A Ya *Prikladnaya Magnitooptika* (Applied Magnetooptics) (Moscow: Energoatomizdat, 1990)
42. Vashkovskii A V, Stal'makhov V S, Sharaevskii Yu P *Magnitostaticheskie Volny v Elektronike Sverkhvysokikh Chastot* (Magnetostatical Waves in the Electronics of Microwaves) (Saratov: Izd. Saratov. Univ., 1993)
43. Ustinov V V et al. *Zh. Eksp. Teor. Fiz.* **109** 477 (1996) [*JETP* **82** 253 (1996)]
44. Kostyuchenko V V, Zvezdin A K *Phys. Rev. B* **57** 5951 (1998)
45. Shutyi A M, Sementsov D I *Fiz. Tverd. Tela* **46** 271 (2004) [*Phys. Solid State* **46** 277 (2004)]
46. Iskhakov R S, Gavrishin I V, Chekanova L A *Pis'ma Zh. Eksp. Teor. Fiz.* **63** 938 (1996) [*JETP Lett.* **63** 989 (1996)]
47. Bebenin N G et al. *Fiz. Met. Metalloved.* **82** (4) 39 (1996) [*Phys. Met. Metallogr.* **82** 348 (1996)]
48. Bebenin N G, Ustinov V V *Fiz. Met. Metalloved.* **84** (2) (1997) [*Phys. Met. Metallogr.* **84** 112 (1997)]
49. Kreines N M, Kolmogorov A N, Mescheriakov V F *J. Magn. Magn. Mater.* **177–181** 1189 (1998)
50. Vedyayev A et al. *Phys. Lett. A* **185** 117 (1994)
51. Bruno P, Chappert C *Phys. Rev. B* **46** 261 (1992)
52. Schreyer A et al. *Phys. Rev. B* **52** 16066 (1995)
53. Men'shov V N, Tugushev V V *Zh. Eksp. Teor. Fiz.* **125** 136 (2004) [*JETP* **98** 123 (2004)]
54. Urazhdin S *Phys. Rev. B* **69** 134430 (2004)
55. Berkov D V, Gorn N L *Phys. Rev. B* **72** 094401 (2005)
56. Kiselev S I et al. *Phys. Rev. Lett.* **93** 036601 (2004)
57. Rezende S M, de Aguiar F M, Azevedo A *Phys. Rev. B* **73** 094402 (2006)
58. Neite B, Dötsch H *Proc. SPIE* **1018** 115 (1989)
59. Shutyi A M, Sementsov D I *Fiz. Tverd. Tela* **43** 1439 (2001) [*Phys. Solid State* **43** 1499 (2001)]
60. Shutyi A M, Sementsov D I, in *Novye Magnitnye Materialy Mikroelektroniki: Sb. Trudov XX Mezhdunar. Shkoly-Seminara, 12–16 Iyunya 2006 g., Moskva* (Proc. XX Intern. School-Seminar on the New Magnetic Materials for Microelectronics, June 12–16, 2006, Moscow) (Moscow: Izd. Fizich. Fak. MGU, 2006) p. 73
61. Zvezdin A K et al. *Fiz. Tverd. Tela* **32** 1812 (1990)
62. Balbashov A M, Chervonenkis A Ya *Magnitnye Materialy dlya Mikroelektroniki* (Magnetic Materials for Microelectronics) (Moscow: Energiya, 1979)
63. Shutyi A M, Sementsov D I *Kristallografiya* **51** 330 (2006) [*Crystallogr. Rep.* **51** (1) 303 (2006)]
64. Fedosyuk V M, Makutin G V, Kasyutich O N *Zarubezh. Radioelektron.* (4–5) 42 (1992)
65. Nosov R N, Sementsov D I *Fiz. Tverd. Tela* **42** 1430 (2000) [*Phys. Solid State* **42** 1471 (2000)]
66. Sementsov D I, Shutyi A M *Pis'ma Zh. Eksp. Teor. Fiz.* **74** 339 (2001) [*JETP Lett.* **74** 306 (2001)]
67. Shutyi A M, Sementsov D I *Fiz. Met. Metalloved.* **95** (3) 5 (2003) [*Phys. Met. Metallogr.* **95** 211 (2003)]
68. Gerrits Th et al. *Phys. Rev. B* **73** 094454 (2006)
69. Sementsov D I, Shutyi A M *Fiz. Tverd. Tela* **45** 877 (2003) [*Phys. Solid State* **45** 922 (2003)]
70. Babushkin I V, Logvin Yu A, Loiko N A *Zh. Eksp. Teor. Fiz.* **117** 149 (2000) [*JETP* **90** (1) 133 (2000)]
71. Sides S W, Rikvold P A, Novotny M A *Phys. Rev. E* **57** 6512 (1998)

72. Demokritov S O et al. *Zh. Eksp. Teor. Fiz.* **122** 1233 (2002) [*JETP* **95** 1062 (2002)]
73. Zvezdin A K, Kostyuchenko V V *Fiz. Tverd. Tela* **39** 178 (1997) [*Phys. Solid State* **39** 155 (1997)]
74. Kurkin M I, Khusainov D Z *Fiz. Tverd. Tela* **41** 660 (1999) [*Phys. Solid State* **41** 595 (1999)]
75. Drovosekov A B et al. *Zh. Eksp. Teor. Fiz.* **116** 1817 (1999) [*JETP* **89** 986 (1999)]
76. Milyaev M A et al., in *Novye Magnitnye Materialy Mikroelektroniki: Sb, Trudov XX Mezhdunar. Shkoly-Seminara, 12–16 Iyunya 2006 g., Moskva* (Proc. XX Intern. School-Seminar on the New Magnetic Materials for Microelectronics, June 12–16, 2006, Moscow) (Moscow: Izd. Fizich. Fak. MGU, 2006) p. 102
77. Bebenin N G, Ustinov V V *Fiz. Met. Metalloved.* **84** (2) 29 (1997) [*Phys. Met. Metallogr.* **84** 112 (1997)
78. Sementsov D I, Shutyi A M *Zh. Tekh. Fiz.* **74** (4) 42 (2004) [*Tech. Phys.* **74** 420 (2004)]
79. Rezende S M et al. *Phys. Rev. B* **55** 8071 (1997)
80. Shutyi A M, Sementsov D I *Fiz. Met. Metalloved.* **97** (2) 24 (2004) [*Phys. Met. Metallogr.* **97** 140 (2004)]
81. Serpico C et al. *J. Magn. Magn. Mater.* **290–291** 502 (2005)
82. Özyilmaza B, Kent A D *Appl. Phys. Lett.* **88** 162506 (2006)
83. Wegrowe J-E *Phys. Rev. B* **68** 214414 (2003)
84. Bebenin N G, Ustinov V V *Fiz. Met. Metalloved.* **89** (3) 19 (2000) [*Phys. Met. Metallogr.* **89** 225 (2000)]
85. Shutyi A M *Radiotekh. Elektron.* **50** 626 (2005) [*J. Commun. Technol. Electron.* **50** 574 (2005)]
86. Schmool D S, Barandiarán J M *J. Phys: Condens. Matter* **10** 10679 (1998)
87. Shutyi A M, Sementsov D I *Fiz. Met. Metalloved.* **99** (5) 31 (2005) [*Phys. Met. Metallogr.* **99** 473 (2005)]
88. Chesman C et al. *Phys. Rev. B* **58** 101 (1998)
89. Meersschaut J et al. *Phys. Rev. Lett.* **87** 107201 (2001)
90. Loskutov A Yu *Vestn. Mosk. Univ., Ser. 3. Fiz., Astron.* (3) 3 (2001) [*Moscow Univ. Phys. Bull.* **56** (3) 1 (2001)]
91. Loskutov A Y, Tereshko V M *Proc. SPIE* **2038** 263 (1993)
92. Loskutov A Yu *Vestn. Mosk. Univ., Ser. 3. Fiz., Astron.* (2) 3 (2001) [*Moscow Univ. Phys. Bull.* **56** (2) 1 (2001)]
93. Blank M L *Usp. Mat. Nauk* **44** (6) 3 (1989)
94. Schuster H *Deterministic Chaos* (Weinheim: Physik-Verlag, 1984) [Translated into Russian: Moscow: Mir, 1988]
95. Berge P, Pomeau Y, Vidal C *L'ordre dans le Chaos. Vers une Approache Deterministe de la Turbulence* (Paris: Hermann, 1988) [Translated into Russian: Moscow: Mir, 1991]
96. Akhromeeva S et al. *Nestatsionarnye Struktury i Diffuzionnyi Khaos* (Nonstationary Structures and Diffusion Chaos) (Moscow: Nauka, 1992)
97. Jeffries C , Perez J *Phys. Rev. A* **27** 601 (1983)
98. Van Buskirk R, Jeffries C *Phys. Rev. A* **31** 3332 (1985)
99. Bertotti G et al. *J. Appl. Phys.* **89** 6710 (2001)
100. Alekseev K N et al. *Usp. Fiz. Nauk* **162** (7) 81 (1992) [*Sov. Phys. Usp.* **35** 572 (1992)]
101. Demidov V E, Kovshikov N G *Pis'ma Zh. Eksp. Teor. Fiz.* **66** 243 (1997) [*JETP Lett.* **66** 261 (1997)]
102. Shutyi A M, Sementsov D I, in *Novye Magnitnye Materialy Mikroelektroniki: Sb. Trudov XX Mezhdunar. Shkoly-Seminara, 12–16 Iyunya 2006 g., Moskva* (Proc. XX Intern. School-Seminar on the New Magnetic Materials for Microelectronics, June 12–16, 2006, Moscow) (Moscow: Izd. Fizich. Fak. MGU, 2006) p. 7
103. Malinetskii G G, Potapov A B *Sovremennye Problemy Nelineinoi Dinamiki* (Modern Problems of Nonlinear Dynamics) (Moscow: Editorial URSS, 2002)
104. Shutyi A M, Sementsov D I *Pis'ma Zh. Eksp. Teor. Fiz.* **78** 952 (2003) [*JETP Lett.* **78** 480 (2003)
105. Lisovskii F V, Polyakov O P *Pis'ma Zh. Eksp. Teor. Fiz.* **73** 546 (2001) [*JETP Lett.* **73** 483 (2001)
106. Robb D T, Reichl L E *Phys. Rev. E* **57** 2458 (1998)
107. Solov'ev M M, Filippov B N *Fiz. Tverd. Tela* **39** 2036 (1997) [*Phys. Solid State* **39** 1821 (1997)]
108. de Aguiar F M, Azevedo A, Rezende S M *J. Appl. Phys.* **91** 8046 (2002)
109. Zhu Xiaochun, Zhu Jian-Gang, White Robert M *J. Appl. Phys.* **95** 6630 (2004)
110. Shutyi A M, Sementsov D I *Fiz. Tverd. Tela* **46** 2006 (2004) [*Phys. Solid State* **46** 2073 (2004)]
111. Sementsov D I, Shutyi A M *Dokl. Ross. Akad. Nauk* **394** 324 (2004) [*Dokl. Phys.* **49** 39 (2004)]